

Robust static estimation from surface wave data

*Original*

Robust static estimation from surface wave data / Socco, Laura; Mabyalaht, Guy; Comina, Cesare. - ELETTRONICO. - (2015), pp. 5222-5227. (Intervento presentato al convegno SEG Annual Meeting tenutosi a New Orleans nel 18-23 Ottobre 2015) [10.1190/segam2015-5837633.1].

*Availability:*

This version is available at: 11583/2620044 since: 2015-12-10T00:00:59Z

*Publisher:*

SEG - Society of Exploration Geophysicists

*Published*

DOI:10.1190/segam2015-5837633.1

*Terms of use:*

This article is made available under terms and conditions as specified in the corresponding bibliographic description in the repository

*Publisher copyright*

(Article begins on next page)

# Analysis of the performance of linear Fresnel collectors: encapsulated vs. evacuated tubes

M. Cagnoli<sup>1</sup>, D. Mazzei<sup>2</sup>, M. Procopio<sup>1</sup>, V. Russo<sup>2</sup>, L. Savoldi<sup>1</sup>, R. Zanino<sup>1</sup>

<sup>1</sup> *Dipartimento Energia, Politecnico di Torino, 10129 Torino Italy*

<sup>2</sup> *ENEA, Centro della Casaccia, 00123 Roma Italy*

\*Corresponding author: [laura.savoldi@polito.it](mailto:laura.savoldi@polito.it)

---

## Abstract

In order to reduce the cost of the produced electricity, the Linear Fresnel Collector (LFC) system is a promising Concentrated Solar Power (CSP) technology. In this paper a detailed study is conducted aimed at the assessment of the heat losses from the receiver of a real 1 MWe pilot plant based on the Fresnel collector and cooled with a thermal oil. The receiver unit, which consists of an absorber tube and a compound parabolic concentrator (CPC), is investigated numerically in order to determine the receiver performance in different wind directions. Two receiver configurations are analyzed: a simply encapsulated one and an evacuated one. In the latter case, high vacuum conditions are reached in the gap between the absorber tube and the glass cover, whereas in the former case, air at ambient pressure fills the gap. The spatial distribution of the heat flux absorbed by the absorber tube and by the glass cover is determined by means of an optical analysis, conducted with the Monte Carlo based open-source ray-tracing tool Tonatiuh, and it is the driver of the ensuing thermal fluid dynamic analysis. A reference operation condition is studied in detail by means of a 1D model that solves the energy balance for the coolant along the entire length of the receiver. The characterization of the 1D model requires an accurate, multi-dimensional computational fluid dynamic (CFD) analysis, based on the commercial STAR-CCM+ code, which aims at determining the useful heat transferred to the coolant and the convective and radiative heat losses as a function of the oil temperature. A 2D CFD model is used to simulate the thermal behavior of the receiver at different locations along its axis in case of no wind or wind blowing across the collector axis. A 3D CFD model is adopted to study the impact of the wind blowing along the collector axis. The external air is considered in the computational domain in both CFD models, to be able to accurately assess the convective share of the heat losses. At the end, the oil temperature profile along the receiver tube, as well as the heat losses and the thermal efficiency trends, are presented and discussed. The 2D model is also exploited to perform an annual analysis, varying the solar flux and the sun position, but considering just a single wind direction. The results of our analysis indicate that the benefit of using an evacuated tube depends on the heat absorbed on the linear receiver, which depends in turn on the solar flux and on the sun position. The annual-based performance improvement obtained using an evacuated tube is not dramatic, due to the relatively low temperatures of the receiver. Moreover, this analysis also concludes that the receiver performance is only slightly affected by the wind direction and intensity up to ~4 m/s, due to the presence of the CPC that protects the receiver from the external air stream.

Keywords: Fresnel, CFD, Monte Carlo method, heat losses, evacuated tube

---

# 1 Introduction

Among line-focusing technologies for Concentrated Solar Power (CSP), the parabolic trough is the current leader, established at commercial level since the 80's (SEGS plants in California, USA).

More recently, the Linear Fresnel Collector (LFC) has been proposed as a cost effective alternative to the parabolic trough technology (Morin et al., 2012; Sait et al., 2015). The cost reduction allowed by the LFCs is due to their constructive simplicity: there are no rotating joints or high-temperature moving components and the support structures are lighter than in case of parabolic collectors (Qiu et al., 2015). The possibility to use lighter structure is in fact a consequence of the low mirrors altitude and wind load (Lancereau et al., 2015).

A LFC system consists of a set of parallel-placed flat or slightly curved mirrors stripes, which focus the solar radiation onto a fixed linear receiver. To minimize the shading and blocking effect due to the adjacent mirrors, the Compact Linear Fresnel technology has been proposed (Mills and Morrison, 2000), which also allows reducing the land usage since the mirrors stripes can be installed very close to each other. This technology employs two receiver lines for each solar field; thus, the mirrors have two possible orientations that allow optimizing the solar field. From a thermal point of view, the LFC is competitive with respect to the more widespread parabolic trough technology. Montes et al. (2016) developed a 2D model based on a thermal resistance scheme to study the thermal behavior of a receiver mounted in a CPC cavity closed at the bottom by a glass plate concluding that the LFC performs better than the parabolic trough in terms of receiver thermal efficiency. Nevertheless, the overall efficiency of the LFCs is lower than the one achieved with the parabolic trough collectors due the poor optical performance of the Fresnel systems. Innovative LFC layouts have been proposed with the aim to overcome the gap in optical efficiency compared with the parabolic trough; as for example in (Canavarro et al., 2014).

Two configurations can be identified for the receiver of the LFC: the single-tube receiver and the multi-tube receiver. The former includes an absorber tube mounted in a cavity consisting of a secondary concentrator, like a Compound Parabolic Concentrator (CPC). The cavity can be closed at the bottom with a glass plate, in order to reduce the radiative (greenhouse effect) and convective losses. As an alternative, the absorber tube can be encapsulated in a glass envelope, see (Grena and Tarquini, 2011; Qiu et al., 2015). Absorber tubes encapsulated in a glass cover are widely used in parabolic trough systems, as they allow evacuating the gap between the absorber and the glass tube. This should lead to a reduction of the convective losses and protect the selective coating of the absorber, since the stability in air of these coatings at high temperatures is still an open issue (Raccurt et al., 2015).

This paper concentrates on a receiver with a single tube configuration, equipped with an encapsulated absorber tube, aiming at studying the radiative and convective heat loss mechanisms that lower the receiver efficiency. According to the current literature, the single tube still represents a promising design for the Fresnel linear receiver, especially because it allows evacuating the absorber tube, which can be a key advantage in terms of heat losses reduction and coating stability. The paper considers both the evacuated and non-evacuated (i.e. simply encapsulated) cases, with thermal oil as the heat transfer fluid (HTF), and the two configurations are compared in terms of performance.

Several projects have been based on the single tube configuration, including the Fresdemo prototype (Bernhard et al., 2008), that was built at the Plataforma Solar de Almeria in Spain to demonstrate the maturity of the LFC technology. Heimsath et al. (2014) numerically investigated the heat losses from a single-tube receiver that employs a CPC cavity with a flat glass cover (glass-plate receiver). The analysis was performed using both a CFD model coupled with a ray tracing code that provided the absorbed heat flux over the secondary concentrator and a faster model based on a thermal resistance scheme. In the CFD model, the absorber tube temperature was imposed and the computational domain didn't include the external air. The main conclusion of this work was that the impact of the heat absorbed by the secondary concentrator cannot be neglected to accurately evaluate the heat losses from a glass-plate receiver. Because of the different receiver design (glass-plate VS encapsulated), this result is not applicable to the cases analyzed in the present paper.

Qiu et al. (2015) investigated the optical and thermal performance of a single-tube receiver with a CPC cavity and an evacuated absorber tube coupling a Monte Carlo ray tracing code with a finite volume model. The results from this study indicated that using cylindrical mirrors instead of parabolic leads to achieve nearly the same performance, but it allows reducing the mirrors cost since the cylindrical shape is easier to be manufactured. In addition, this work concluded that the heat losses strongly depend on the temperature difference between the coolant and the ambient,

while they are weakly influenced by the DNI (Direct Normal Irradiance) level (where the radiation is always assumed at normal incidence) since most of the heat is in any case transferred to the HTF, and namely molten salts. Thanks to the vacuum in the gap, they found that the thermal efficiency is always above 70%.

Recently, Montes et al. (2017) compared different single-tube receiver designs using numerical thermal resistance models; all the designs considered were equipped with a CPC secondary concentrator. This study concluded that the best thermal performance is obtained using an evacuated absorber tube, followed by the glass-plate receiver, where the absorber tube is not encapsulated, but the cavity is closed at the bottom with a flat glass, and finally by the nude receiver, where the absorber tube is not encapsulated and the cavity is exposed to the environment. However, the performance differences among these designs becomes quite negligible if the absorber temperatures is low enough. For this reason, they proposed a hybrid configuration, which employs a nude receiver in the first modules (low temperature), while it adopts an evacuated absorber tube for the remaining modules at higher temperature. With respect to the work of Montes et al. (2017), in this paper the simply encapsulated absorber tube is studied instead of the nude tube and the effect of the wind direction is investigated by means of an innovative modeling approach.

The multi-tube receiver consists of an array of parallel absorber tubes arranged in a trapezoidal cavity that can be closed at the bottom with a flat glass. This receiver design has the advantage of a larger absorber area with respect to the single-tube configuration; however, there is no clear winner in terms of receiver performance between these two designs on the base of the current literature.

A number of works have been carried out to study the heat losses from a multi-tube receiver equipped with a trapezoidal cavity. According to (Qiu et al., 2016; Sahoo et al., 2013), the radiation mechanism dominates the heat transfer from the cavity to the external ambient; thus, the coating emissivity, which has to be kept as low as possible, plays a key role in reducing the heat losses. Based on that, the role of the radiative, as opposed to convective, losses will be investigated in the present paper on the receiver configuration considered here, and a parametric study will also be performed to investigate the effect of the coating emissivity.

Moghimy et al. (2015) considered a trapezoidal cavity provided with an array of parallel absorber tubes to demonstrate how to use the CFD commercial software ANSYS Fluent, based on the finite volume method, to perform both the ray trace analysis (2D model) needed to compute the absorbed heat and the conjugate heat transfer analysis (3D model). The accuracy of the optical model, which exploits the discrete ordinates method, was proved comparing the results with the ones obtained using a Monte Carlo ray tracing code.

As stated before, the aim of this paper is to estimate accurately the heat losses that occur from the absorber tube to the external ambient. A common approach available in the literature to perform such an analysis is to study the thermal behavior of the receiver unit (absorber tube + cavity) performing a Computational Fluid Dynamic (CFD) analysis, see for example (Haberle et al., 2002; Moghimy et al., 2015; Qiu et al., 2015, 2016). In these analyses, the coolant is included in the computational domain and a fixed heat transfer coefficient is assumed to compute the convective heat losses towards the external ambient. Other studies use 1D lumped models to predict the receiver behavior; these models are based on thermal resistance schemes and they typically calculate the convective heat losses by means of heat transfer correlations, e.g. (Heimsath et al., 2014; Montes et al., 2017, 2016; Singh et al., 2010).

In this paper a novel CFD-based approach has been adopted, which aims at estimating the convective heat flux towards the external ambient in a more accurate way. To do this, the actual interaction between the external air flow and the real geometry of the receiver unit has been simulated by means of a steady-state CFD model, considering both natural convection and different wind conditions. The computed convective losses are then used to feed a 1D model that allows the evaluation of the global efficiency of the Fresnel line. This method has been applied to investigate a reference operation condition (fixed day/time) in a detailed way, while the influence of the DNI level and of the sun position has been assessed simulating different days and times during one year, limiting the parameter space to a single wind direction in order to keep an acceptable computational cost. The adopted approach allows, as a byproduct, the evaluation of the suitability of the correlations used in literature to compute the convective losses, and the extension of the 1D model also in the conditions (e.g. different wind directions) out of the correlations validity range.

## 2 Reference Fresnel plant

We concentrate our analysis here on a 1MW<sub>e</sub> CSP-ORC pilot plant based on Fresnel collectors, under construction at the Green Energy Park in Morocco (IRESEN, 2016), in view of the availability of data on the system geometry and materials. Since this work concerns the solar field and mainly focusses on the receiver unit, a short description of the linear receiver installed in the reference plant is here provided.

According to (Soltigua, 2015), the solar field of the pilot plant considered consists of 7 identical hydraulics loops, which are placed in parallel, see Figure 1. Each loop is composed by 4 Linear Fresnel Collectors (model FLT10v produced by Soltigua), which are of the standard type, i.e. the Compact Linear Fresnel technology is not adopted here. The total length of the loop is about 270 m with a net collecting surface of about 1600 m<sup>2</sup>; the hydraulic loops have a “U-shape”, as shown in Figure 1. Hence, the inlet and outlet of the working fluid, which is a thermal oil (DelcoTerm Solar E15), are on the same side. The orientation of the solar field is 17.7° from the North-South (N-S) direction. Although the N-S alignment ensures the best optical performance, the available land at the plant site only made possible to install the solar field with the mentioned orientation.

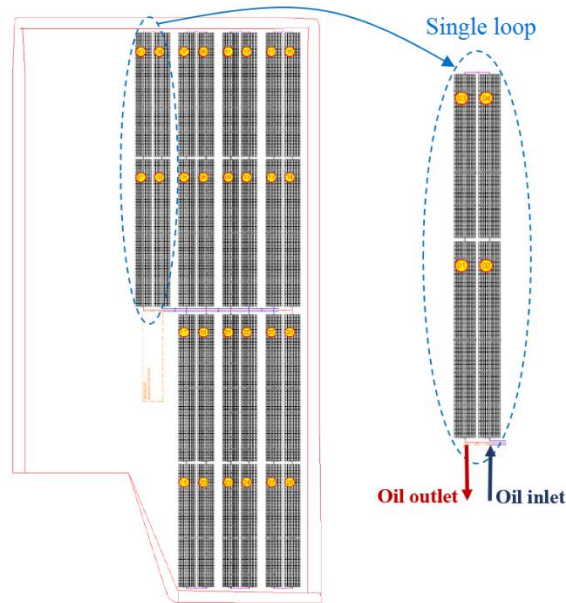


Figure 1 – Solar Field of the 1 MW<sub>e</sub> pilot plant at the Green Energy Park (Morocco) which consists of 7 loops (Soltigua, 2015). The zoom shows a single loop, while the yellow bullets identify the four Soltigua FLT10v collectors (01-04) in each loop.

The FLT10v collector is made of a number of basic modules consisting of 10 parallel mirrors rows, each including 4 mirrors in series, and a receiver unit that includes an encapsulated absorber tube and a secondary concentrator of CPC type (see Figure 2). The width of each basic module is about 8 m, while the length is about 6 m. The main features of the mirror field are summarized in

Table 1.

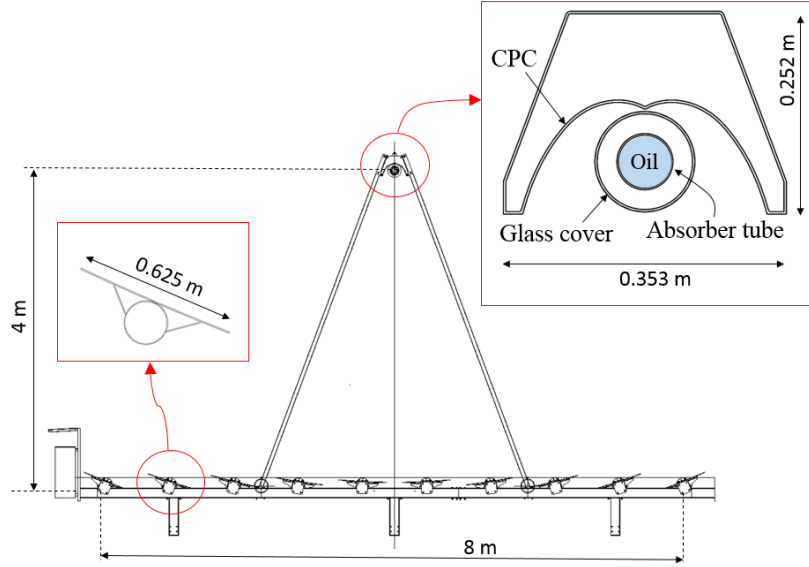


Figure 2 – A lateral view of the Soltigua FLT10v Fresnel collector with a zoom on the single mirror and on the receiver unit (ENEA, 2015; Soltigua, 2015)

Table 1 – Description of the mirror field, w.r.t. the basic module of the FLT10v collector (ENEA, 2015)

Parameter	Value
Number of parallel mirror rows	10
Length of basic module	6.17 m
Width of the single mirror	0.625 m
Width of the mirror field	8.05 m
Mirror cross section shape	Cylindrical

The encapsulated absorber tube, manufactured by ASE - Archimede Solar Energy, is mounted 4 m above the mirrors and its geometric characteristics are summarized in Table 2. A selective coating (CERMET) is applied on the outer surface of the absorber tube (ENEA, 2015). The FLT10v basic modules are equipped with an evacuated absorber tube (pressure in the annulus  $\approx 10^{-4}$  mbar (ENEA, 2015)). However, the not-evacuated (simply-encapsulated) configuration is also analyzed in this paper, to estimate the difference between the two options in terms of performance. Also the simply-encapsulated option in fact turns out to be realistic, in view of the relatively low operating temperature of the LFC system here analyzed ( $< 300^\circ\text{C}$ ), at which some selective coatings showed a good stability in air (Raccurt et al., 2015). In the reference conditions (see Table 3), each parallel loop generates about  $0.7 \text{ MW}_{\text{th}}$ , increasing the temperature of the heat transfer fluid from about  $180^\circ\text{C}$  (453 K) to  $300^\circ\text{C}$  (573 K), according to the turbine requirements, which is designed to expand the working fluid from  $300^\circ\text{C}$  to  $180^\circ\text{C}$ . The power unit exploits then an Organic Rankine Cycle (ORC) to convert the heat carried by the thermal oil into electricity.

Table 2 – Geometric features of the receiver tube (ENEA, 2015)

Parameter	Value
Absorber tube outer diameter	0.070 m
Absorber tube thickness	0.002 m
Glass cover tube outer diameter	0.125 m
Glass cover tube thickness	0.003 m

Table 3 – Reference conditions for the 1 MW<sub>e</sub> pilot plant as defined in (Soltigua, 2015)

Parameter	Value
Reference day	March 21 <sup>st</sup>
Reference time	GMT 12:00
Direct Normal Irradiance (DNI)	850 W/m <sup>2</sup>
Ambient temperature (dry bulb)	303 K (30°C)
Relative humidity	30 %
Ambient pressure	952 mbar
Wind speed	3.7 m/s
Direction of the wind	North-South

### 3 Modeling approach

As mentioned above, two receiver configurations are addressed in the present paper:

- Encapsulated and evacuated;
- Simply encapsulated (non-evacuated).

For both configurations, the receiver performance is evaluated in terms of solar-to-thermal efficiency and temperature reached by the working fluid at the outlet section of the collector string in reference (steady-state) conditions, following the procedure summarized in Figure 3.

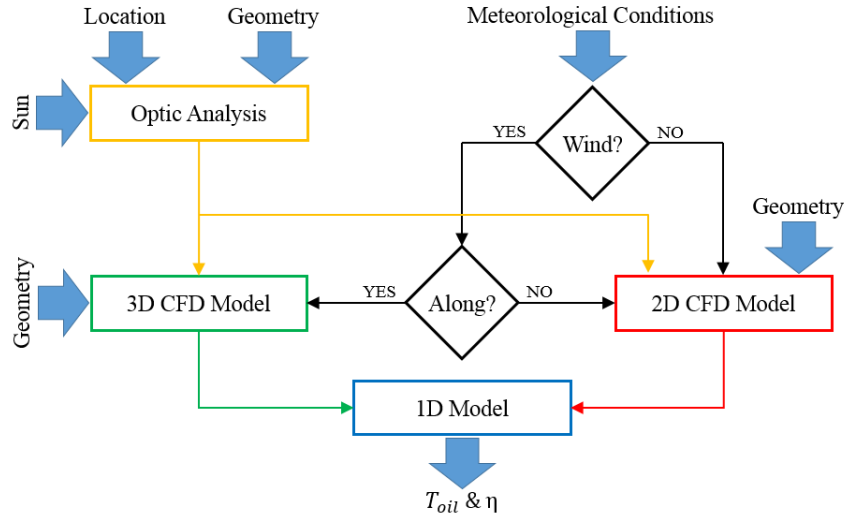


Figure 3 – Scheme of the numerical procedure implemented to evaluate the receiver performance in different wind conditions

Taking advantage of the fact that all cooling circuit loops are in parallel, see Figure 1, we consider a 1D model (in the direction of the absorber axis) of a single loop, as the simulation of the entire hydraulic loop with a 3D CFD model is not viable, in view of the high computational cost. This model solves the steady-state energy balance equation for the working fluid, which is driven by the heat flux transferred to the thermal oil.

The aim of the steady-state 1D model is to evaluate the oil temperature profile along the receiver axis. For this purpose, the entire length of the single hydraulic loop has been discretized in finite volumes, see Figure 4, and the steady-state enthalpy jump is calculated in each volume using an upwind scheme, according to

$$q'_{fluid,i} = \dot{m} \cdot \frac{\Delta h_i}{\Delta z} = \dot{m} \cdot \tilde{c}_{p,i} \cdot \frac{\Delta T_i}{\Delta z} \quad (1)$$

where  $q'_{fluid,i}$  is the useful heat flux, in W/m, transferred to the thermal oil in the volume  $i$ ,  $\dot{m}$  is the oil mass flow rate and  $\Delta h_i$  is the enthalpy jump across the same volume and  $\Delta z$  is the axial length of the finite cylindrical volume. The enthalpy jump can be expressed as a function of the average specific heat ( $\bar{c}_{p,i}$ ) and of the oil temperature difference between the volume outlet/inlet ( $\Delta T_i$ ).

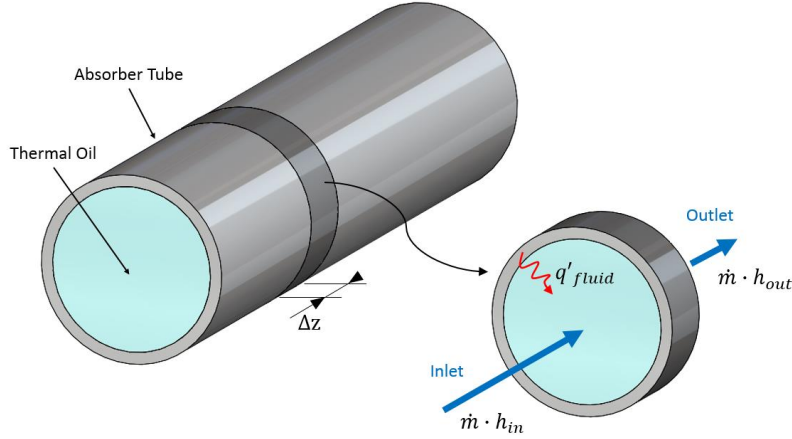


Figure 4 – Scheme of the 1D model with the terms of Eq. 1 highlighted

A good approximation of the oil temperature distribution along the receiver tube can be determined with this simple 1D model only if an accurate description of the heat transfer between the fluid and the environment is provided. The thermal power per unit length transferred to the fluid is given by the difference between the solar flux absorbed by the absorber tube ( $q'_{abs}$ ) and the heat flux transferred to the environment ( $q'_{loss}$ )

$$q'_{fluid} = q'_{abs} - q'_{loss} \quad (2)$$

To evaluate  $q'_{abs}$ , an optical analysis has been conducted using a Monte Carlo based ray-tracing software, which is described in section 4.

The absorbed heat distribution is then exploited as a thermal driver in the CFD models to compute the thermal losses  $q'_{loss}$ , see section 5 below, and, consequently, the heat transferred to the working fluid.

#### 4 Heat flux to the receiver: optical analysis

The absorbed heat flux distribution is the most important driver of the thermal model, and it strongly affects the receiver performance. Therefore, an accurate optical analysis has been conducted using the Monte Carlo based ray-tracing software Tonatiuh (Blanco et al., 2005, 2010) to compute  $q'_{abs}$  simulating the multiple reflections, scatterings and absorptions that occur within the LFC system. The Monte Carlo ray-tracing approach has been widely used in the literature to accurately determine the heat flux absorbed on solar receivers, and proven to provide reliable results in the CSP context, see for example (Qiu et al., 2015).

Since Tonatiuh works under the assumption of elastic collisions, the energy is transferred to a certain surface only if the photon is absorbed by it. Therefore, the energy flux deposited on a certain surface can be easily calculated from the amount of absorbed photons. The heat flux distribution has been evaluated on the absorber tube and on the glass envelope outer surfaces. The heat absorbed on the CPC surface has been neglected in view of the high reflectivity of this surface ( $\approx 90\%$ ). In this way the temperature of the CPC surface turns out to be slightly underestimated and consequently the heat transfer by radiation between the receiver tube and the CPC surface is slightly overestimated (conservative assumption).

The optical analysis has been conducted considering the reference conditions reported in (Soltigua 2015) and defined in Table 3, i.e. March 21<sup>st</sup> at 12:00 GMT, with DNI = 850 W/m<sup>2</sup>, and the actual plant location that in terms of latitude and longitude corresponds to 32.129 N and 7.983 W, respectively.

Figure 5 shows the mirror field simulated in Tonatiuh. It consists of a portion of the entire field, i.e. to a basic module of the FLT10v collector.

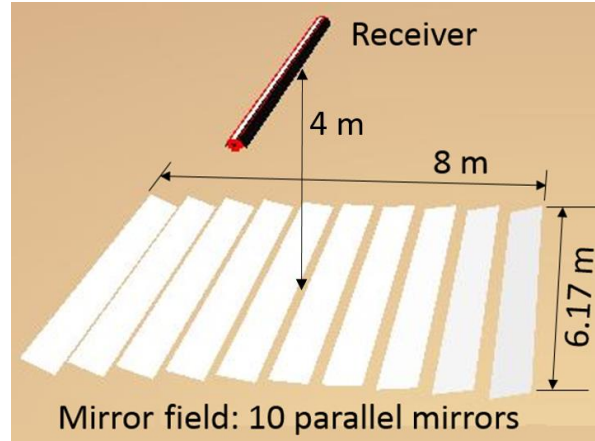


Figure 5 – The LFC system as simulated in Tonatiuh

The geometry of the simulated system is described in Table 1 and Table 2.

The only difference with respect to the actual collector geometry is that each mirror row, which consists of 4 mirrors placed in series, is simplified considering just a single mirror of equivalent length.

The secondary concentrator has been modeled starting from the CAD of the producer. Figure 6 shows the parameters used to define the CPC shape in Tonatiuh, (their values are given in Table 4).

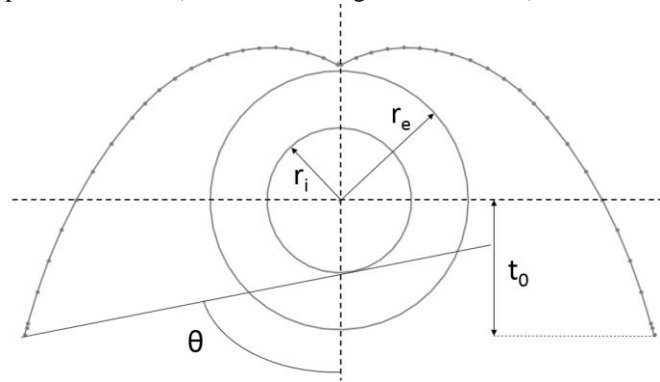


Figure 6 – Parameters to be set defining the CPC profile

Table 4 – Values of the parameters set to define the CPC profile

Parameter	Symbol	Value
Absorber tube external radius	$r_i$	0.0350 m
Glass cover external radius	$r_e$	0.0625 m
Acceptance angle	$\theta$	0.778 rad
Truncation origin	$t_0$	0.065 m

In Table 5, the optical properties of the materials set in Tonatiuh are listed. Note that the optical features of the absorber tube are given by the selective coating applied on its outer surface. Regarding the slope deviation for the reflecting surfaces, the value adopted has been determined in a previous study on a similar Fresnel system (Sabatelli et al., 2013). Only the non-evacuated receiver typology has been analyzed. In fact, the optical model does not change with the receiver configuration, apart from the different transmissivity in the gap between the absorber tube and the glass cover. This region has been simulated in Tonatiuh assuming the default atmospheric transmissivity.

Table 5 – Optical properties of the system components (ENEA, 2015; Sabatelli et al., 2013)

Parameter	Mirrors	Glass cover	Absorber tube	CPC
Reflectivity	0.94	0.00	0.05	0.90
Absorptivity	0.06	0.04	0.95	0.10
Transmissivity	0.00	0.96	0.00	0.00
Refractive index	-	1.43	-	-
Slope deviation (mrad)	5	-	-	5

The post-processing of the computed photon absorption distribution allows determining the absorbed heat flux maps on the surfaces of interest. Starting from the outer surface of the absorber tube, a sensitivity analysis has been performed to make sure that the final results are independent from the number of the simulated photons. The results of this analysis indicate that  $6 \times 10^7$  photons are enough to obtain a heat flux distribution independent on the number of photons retained in the analysis. According to Figure 7a, the heat flux distribution is essentially 2D, as expected, since no remarkable changes occur along the absorber tube axis. Therefore, the main interest is on the azimuthal heat flux distribution, see Figure 7b.

Figure 7b highlights the presence of three peaks in the azimuthal heat flux distribution. The highest one is on the bottom side and is due to the direct concentrated solar radiation from the mirror field. The two peaks in the upper part, which are more or less symmetrical, correspond to the focuses of the parabolic concentrators of the CPC unit. The average solar flux absorbed on the absorber tube surface is equal to  $15.9 \text{ kW/m}^2$ .

Moving to the glass envelope, a larger number of photons (0.9 billion), are needed to ensure the independence of the results on the number of photons. In fact, the glass cover has a very high transmissivity (see Table 5), then a small number of the photons reaching the glass surface are absorbed on it, requiring a larger number of total photons to obtain a good statistics, compared to the case of the absorber tube.

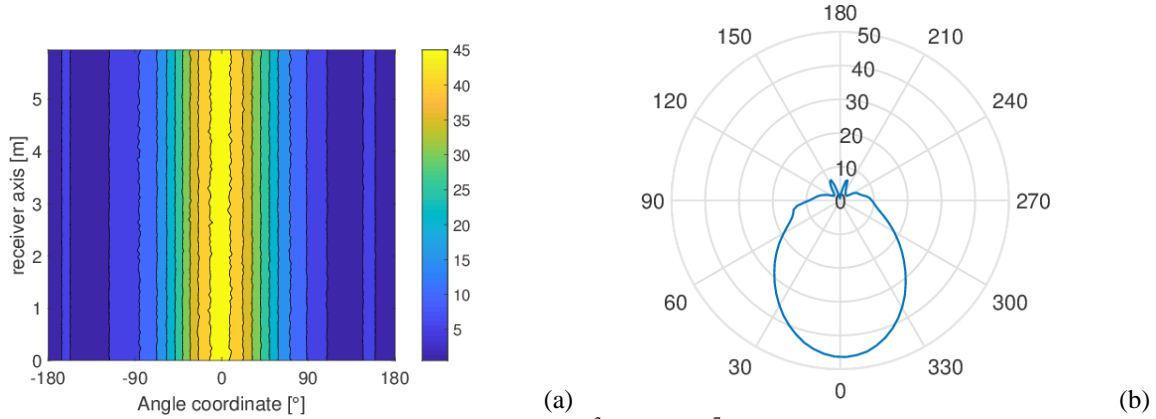


Figure 7 – Heat flux distribution on the absorber tube, in  $\text{kW/m}^2$ , with  $6 \times 10^7$  photons simulated, (a) heat flux map and (b) corresponding azimuthal distribution

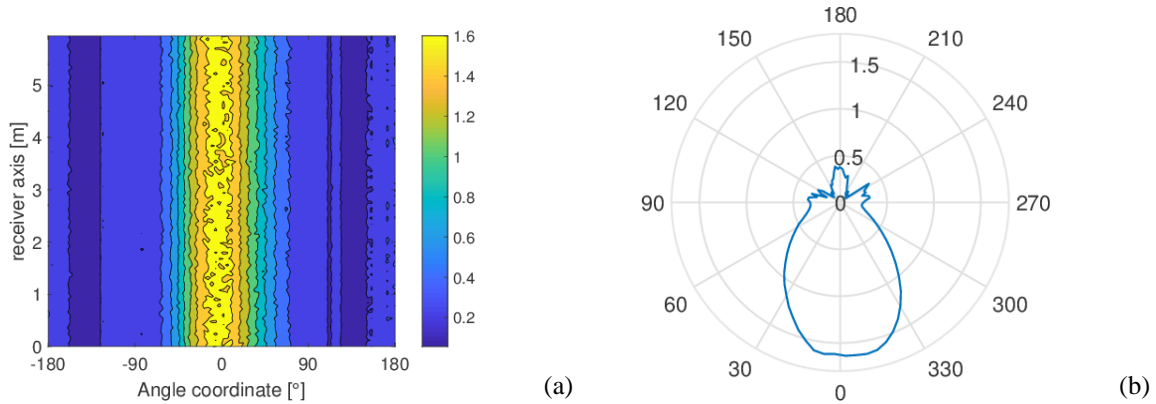


Figure 8 – Heat flux distribution on the glass envelope, in  $\text{kW/m}^2$ , with  $9 \times 10^8$  photons simulated, (a) heat flux map and (b) corresponding azimuthal distribution

Looking at Figure 8a, the heat flux distribution on the glass envelope is again essentially 2D, as expected. The azimuthal heat flux distribution is shown in Figure 8b. Similarly to the absorber tube case, also the heat absorbed on the glass cover presents a very pronounced peak on the bottom side, while smaller peaks can be observed on the upper side due to the solar rays concentrated by the CPC. The average solar flux absorbed on the glass envelope surface is about  $0.56 \text{ kW/m}^2$ , i.e. much smaller than the one absorbed on the absorber tube, as it was expected due to the high transmissivity of the glass.

#### 4.1 Annual optical performance

The annual profile of the optical efficiency  $\eta_{opt}$ , defined as,

$$\eta_{opt} = Q_{abs} / (DNI \cdot w) \quad (3)$$

where  $Q_{abs}$  is the power absorbed by the absorber tube in  $[\text{W/m}]$ ,  $DNI$  is the Direct Normal Irradiance and  $w$  is the sum of the mirror widths, has been evaluated during the year considering the 4 reference days and the 5 different hours for each day (from 9:00 to 17:00) with the Tonatihu model previously described.

The days considered here are the only one for which the DNI data measured at the plant site are available (Soltigua, 2015); specifically, the DNI levels for the days/hours considered are shown in Figure 9a. The results of this analysis are shown in Figure 9b: the resulting average optical efficiency is about 51%. The actual optical efficiency of the entire solar field could be lower since the Tonatihu model does not account for the tracking error and the cleaning state of the mirrors. Moreover, the shadowing effect due to the neighboring loops (see Figure 1) is not taken into account and the border effect at the beginning/end of the Fresnel lines is neglected.

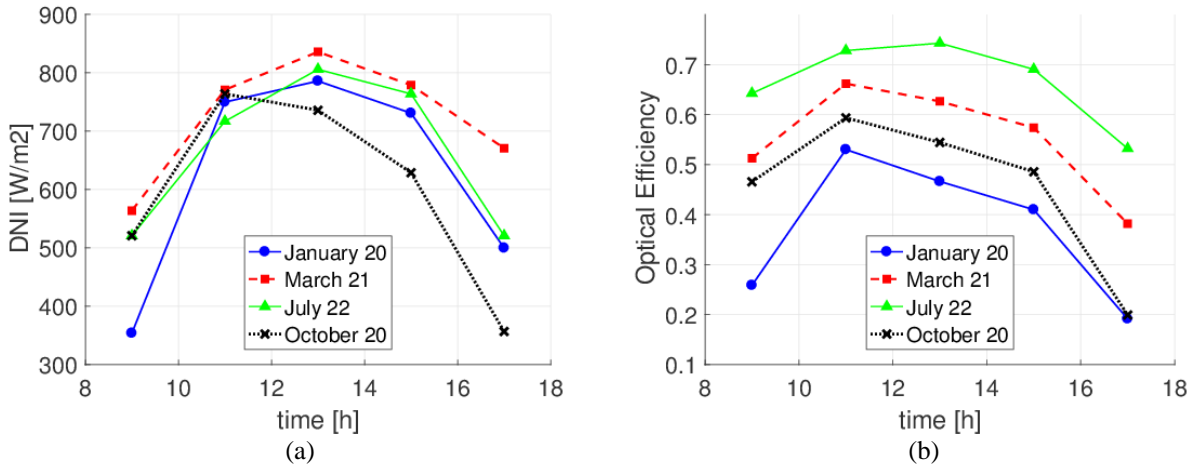


Figure 9 – (a) DNI data for the reference days at the hours considered, and (b) optical efficiency computed with the Tonatihu model during the day (from 9:00 to 17:00) (Soltigua, 2015) .

According to Figure 9b, the optical efficiency changes significantly on the base of the season and of the hour of the day, best performance are reached in the summer period, as expected, between 10:00 and 13:00. The orientation of the solar field, which does not coincide with the N-S direction, as already mentioned, contributes to reduce the symmetry between the morning and the afternoon.

The heat fluxes absorbed on the glass cover and on the absorber tube have been determined post-processing the Tonatihu model for each simulated day/hour, in order to drive the CFD 2D model that is then exploited to study the receiver thermal behavior during the year, see section 5.1.6, using thus a different strategy with respect to Moghimi et al. (2015).

## 5 CFD models of the heat losses from the receiver

The two CFD models (2D and 3D respectively) developed using the commercial CFD software Star CCM+ to compute the heat losses from the receiver solve a steady-state conjugate heat transfer problem, which includes the convective and radiative heat fluxes exchanged within the receiver unit and between the receiver unit and the external air.

The external air flow (wind) obviously has to be included in these models, together with natural convection, in order to accurately determine the convective share of the heat losses from the receiver unit. Depending on the wind direction, two approaches have been adopted in this paper to compute the heat losses and consequently the heat transferred to the fluid:

- In the case of no wind, or of wind direction normal to the receiver axis, a 2D model (on planes perpendicular to the receiver axis) is developed to simulate the receiver behavior at different oil temperatures. Then a correlation is derived between the thermal power per unit length transferred to the working fluid and the temperature difference between the oil and ambient, which will be finally exploited in the 1D model.
- In the case of wind direction parallel to the receiver axis, a 3D CFD model is developed to estimate the wind effect on a small portion of the entire receiver length, close to the leading edge, i.e. the boundary of the receiver unit that is first hit by the air flow. Indeed, there is no need to simulate the entire length of the receiver in this case, since the influence of the wind on the convective losses reduces moving away from the leading edge, up to a distance from which it can be just considered equal to a small fraction of the heat losses without wind (see section 5.1.5).

### 5.1 2D CFD model

#### 5.1.1 Case of no wind

The 2D steady-state model is suitable in the case of no wind conditions and of wind direction normal to the receiver axis.

The computational domain, see Figure 10, includes the external air, CPC unit, with the air volume inside the unit, the glass envelope, the gap between the absorber tube and the glass cover and the absorber pipe (see above for geometry and dimensions of the receiver unit). The external air domain corresponds to a square with 2m long edge. The oil region inside the absorber tube has not been simulated, in order to reduce the computational cost.

Both the evacuated and non-evacuated receiver configurations have been studied with the 2D CFD model. Only the way to model the gap of the encapsulated tube changes:

- In the case of simply encapsulated (non-evacuated) tube, the gap region is filled with air at ambient pressure and temperature (see Table 3), treated as an ideal gas.
- In the case of evacuated tube the gap region is still filled with air at ambient pressure and temperature, but the air thermal conductivity is artificially reduced, in order to approximate the vacuum condition. The idea is to make the convective heat transfer between the absorber tube and the glass envelope negligible, similarly to what is typically done in the lumped parameter models, where a very low heat transfer coefficient is adopted to reach this goal (see section 5.1.4). The imposed thermal conductivity is  $\approx 10^{-6}$  W/mK, which is a value already adopted in the literature to simulate evacuated regions (Weerasinghe and Hughes, 2015).

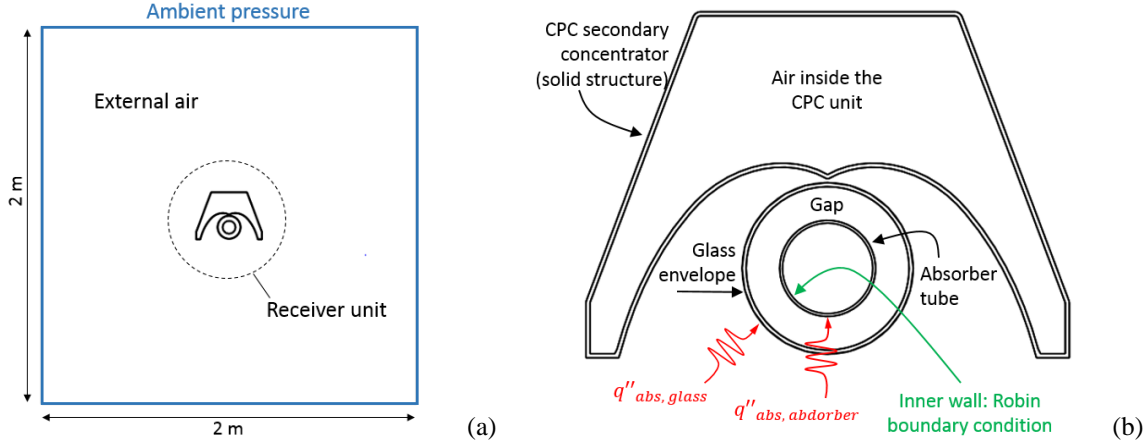


Figure 10 – Computational domain, boundary conditions (see also Table 6) and thermal drivers for the 2D model in the absence of wind: whole domain (a) and a detail of the receiver unit (b). In addition, the different simulated regions are identified.

The boundary conditions and the thermal drivers applied in the model, in the case of no wind, are listed in Table 6, but see also Figure 10.

Concerning the boundary condition imposed on the inner wall of the absorber tube, three different temperatures of the thermal oil in the operational range of the plant have been considered, namely the nominal inlet temperature, i.e., 453 K, the desired outlet temperature, i.e. 573 K, and the mean temperature between the nominal inlet and outlet values (i.e. 513 K)

The convective heat transfer coefficient  $h$  to the thermal oil, needed to define the Robin boundary condition prescribed on the inner wall, has been calculated from the Gnielinski correlation for the Nusselt Number  $Nu$

$$Nu = \frac{(f/8) \cdot (Re - 1000) \cdot Pr_1}{1 + 12.7 \cdot \sqrt{(f/8)} \cdot (Pr_1^{2/3} - 1)} \cdot \left(\frac{Pr_1}{Pr_2}\right)^{0.11} \quad (4)$$

with

$$f = (1.82 \cdot \log_{10}(Re) - 1.64)^{-2} \quad (5)$$

according to (Forristall, 2003), where the inner diameter of the absorber tube is adopted as characteristic length in the definition of  $Nu$ . In Eq. 4,  $Re$  is the Reynolds Number,  $Pr_1$  is the Prandtl Number evaluated at the oil temperature, while  $Pr_2$  is the Prandtl Number evaluated at the temperature of the absorber tube inner wall. The term  $f$  is the friction factor for the inner surface of the absorber pipe, given by Eq. 5. The Gnielinski correlation works in the range of  $Re$  between 3000 and  $5 \times 10^6$  and in the range of  $Pr_1$  between 0.5 and 2000 (Incropera et al., 2012).

To check the validity of this correlation in our case, the dimensionless numbers of interest have been calculated at the oil inlet and outlet sections (nominal oil temperatures 453 K and 573 K respectively). The results indicate that  $Re$  ranges in the interval  $4.5 \times 10^4$ –  $1.2 \times 10^5$  and  $Pr_1$  between 18 and 9, assuming an oil mass flow rate equal to 2.2 kg/s that is the value corresponding to the reference conditions of the pilot plant, according to (Soltigua, 2015). Therefore, the Gnielinski correlation should work properly in the case examined.

Table 7 summarizes the material properties adopted in the CFD model. The glass cover is not assumed to be completely opaque to the thermal radiation; a transmissivity equal to 0.11 has been considered on the base of Kirchhoff's law, according to the thermal emissivity indicated in Table 7. The air regions (the external air, the volume inside the CPC unit and the air in the gap of the encapsulated tube) have been modeled using the ideal gas approximation and assuming that they are transparent to the thermal radiation.

The SST  $k-\omega$  (Menter) turbulence model (Menter, 1994) has been adopted in the external air region and in the air region inside the CPC, which is suitable to study air flows around complex shapes (CD-ADAPCO, 2014). In the gap region, the Realizable  $k-\epsilon$  turbulence model (Shih et al., 1994) has been used, following (Francis et al., 2002). In addition, the gravity effect (buoyancy) has been considered in all the air regions simulated.

In order to numerically solve the thermal-hydraulic problem, the computational domain has been discretized with a grid consisting of polygonal cells. Figure 11 shows a view of the grid generated for the case without wind. The minimum number of cells to obtain grid-independent results turned out to be about  $6 \times 10^4$ .

Table 6 – 2D model: boundary conditions

Location	Description of the boundary conditions
Borders of the external air domain	Imposed ambient pressure and temperature, see Table 3 - “stagnation inlet” boundary condition , as in (CD-ADAPCO, 2014)
Inner wall of the absorber tube	The convective heat transfer with the oil flow, at fixed temperature, has been set, imposing a proper heat transfer coefficient.

Table 7 – Material properties implemented in the CFD model (AK Steel, 2016; CENER, 2015a, 2015b; ENEA, 2015)

Component	Material	$k$ [W/mK]	$\rho$ [kg/m <sup>3</sup> ]	$c_p$ [J/kgK]	Emissivity ( $\epsilon$ )
Absorber tube	AISI 321	20	8027	500	$\epsilon = 0.07513 + 2.2 \times 10^{-7} T_{abs}^2 [^{\circ}C]$
Glass envelope	Borosilicate glass	1.1	2230	850	$\epsilon = 0.89$
CPC	Reflective aluminum	237	2702	903	$\epsilon = 0.1$
Air regions	Air (ideal gas)	0.026	1.086	1003.6	Transparent gas
Vacuum	Air (ideal gas)	$10^{-6}$	1.086	1003.6	Transparent gas

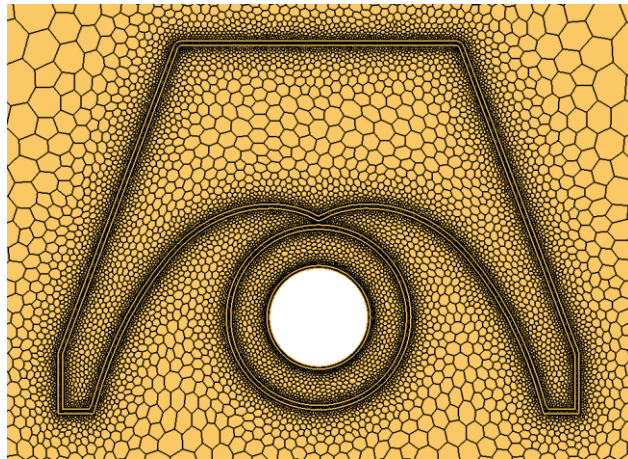


Figure 11 – Mesh used for the 2D CFD analysis in the absence of wind (zoom around the receiver unit)

In Figure 12, the computed velocity field around the receiver unit is shown in the absence of wind, for both the receiver configurations studied here, for an oil temperature equal to 513 K. Of course they are both left-right symmetric, because of the roughly symmetric load conditions. The expected natural convective motions around the glass envelope and below the CPC unit can be observed. No significant difference can be observed comparing Figure 12a and Figure 12b, because the temperature reached by both the glass envelope (see Figure 13) and the CPC surface, does not change significantly with the receiver configuration. In particular, the average temperature of the glass cover is only about 25 K lower in the case of evacuated tube, i.e. ~12% of the total temperature difference between ambient and oil temperature.

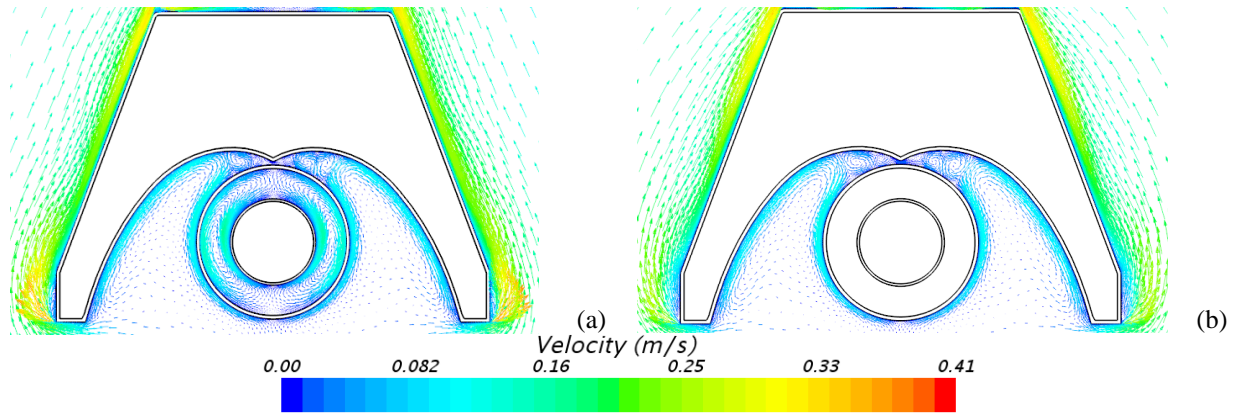


Figure 12 – Velocity field computed around the receiver unit in the absence of wind, assuming  $T_{oil} = 513$  K in case of (a) encapsulated and (b) evacuated tube, respectively.

The relatively small difference between the average temperature computed for the two cases can be explained observing that the heat flux coming from the mirrors and directly absorbed by the glass envelope obviously does not change with the receiver configuration. The average magnitude of this heat flux ( $\sim 220$  W/m) is higher than the average heat transferred from the absorber tube to the glass cover (@ 513 K  $\sim 154$  W/m in the simply encapsulated case and  $\sim 56$  W/m in the evacuated case). Note that the glass envelope absorbs only a share of the radiative heat flux coming from the absorber tube since the glass is partially transparent to the thermal radiation. Therefore, the temperature of the glass envelope is strongly affected by the heat flux directly absorbed on the glass cover itself.

The temperature peaks on the glass envelope in Figure 13 correspond to the peaks of the azimuthal distribution of the absorbed heat flux; see Figure 8b. Comparing Figure 13a and Figure 13b, no significant variations can be observed in the qualitative temperature distribution, only a relatively higher temperature difference between the upper half and the bottom half of the glass cover can be noticed in the simply encapsulated case. This is due to the temperature distribution of the air inside the gap, which is hotter in the upper part due to the free convection; see Figure 14a. Globally, the average temperature of the glass cover changes modestly between the two tube configurations ( $\sim 411$  K in the simply encapsulated case vs.  $\sim 385$  K in the evacuated case).

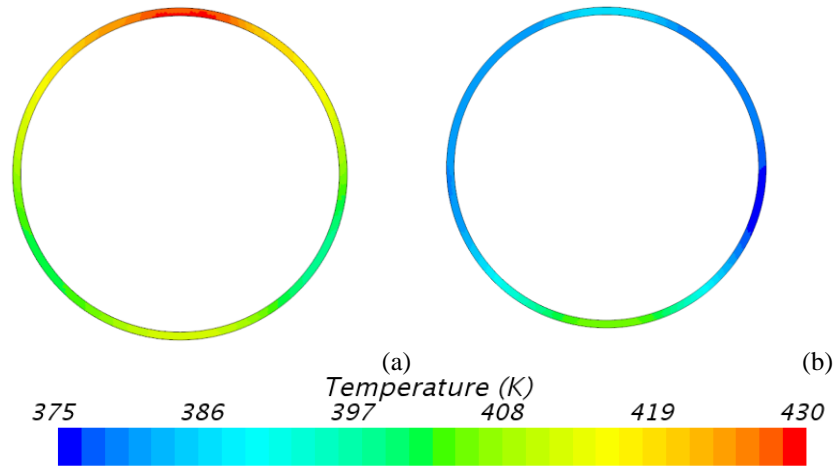


Figure 13 – Temperature distribution computed on the glass envelope in the absence of wind, assuming  $T_{oil} = 513$  K in case of (a) simply encapsulated and (b) evacuated tube, respectively.

Figure 14 shows the temperature field of the simulated regions around the receiver unit for both the analyzed configurations. The external air temperature field does not change significantly in the two cases, due to the small changes in the temperatures of the glass cover and of the CPC surface, as discussed above. The CPC unit prevents the

hot air to easily leave the receiver unit upward, keeping the external air under the secondary concentrator hotter than in the rest of the external air domain.

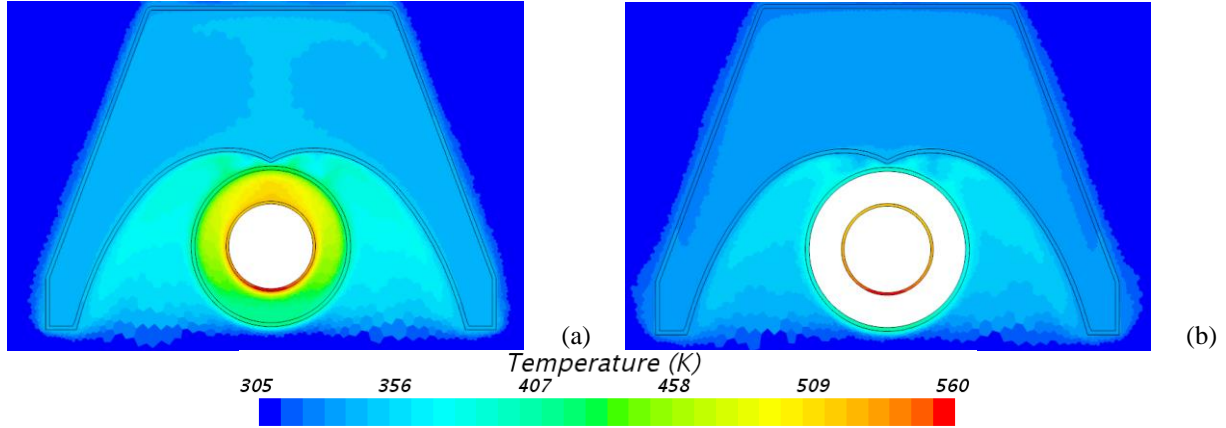


Figure 14 – Air temperature field computed around the receiver unit in absence of wind, assuming  $T_{oil} = 513$  K in case of (a) simply encapsulated and (b) evacuated tube, respectively.

#### 5.1.1.1 Validation against experimental data

In (CENER, 2015b) an experimental campaign is described, conducted to estimate the performance of a 4 m long evacuated tube, like the one used in the reference plant considered in this paper. Those tests were performed heating the absorber tube by means of electric heaters, until a steady-state condition with uniform temperature distribution on the absorber tube and on the glass cover was reached, measuring the temperatures reached by the absorber tube and by the glass cover and the power provided to keep the absorber at constant temperature. In steady-state conditions, this power corresponds to the thermal losses from the absorber tube.

The experimental data can be used to validate the 2D thermal model of the evacuated tube in the case of the absence of wind. However, some relevant differences can be detected between the 2D thermal model and the experimental setup:

- The thermal driver in the tests is not the absorbed solar radiation, which involves both the absorber tube and the glass cover and induces an azimuthally non-uniform temperature distribution.
- The convective heat transfer between the absorber tube and the thermal oil was not present in the experiments.
- In the experiment, the secondary concentrator was not present.

In order for the computational model to be representative of the setup of the experimental campaign, the heat flux absorbed by the glass cover has been removed and the temperature of the absorber tube has been imposed as a thermal driver. Then, the CPC unit has been removed from the computational domain. The external air temperature has been imposed equal to that measured in the experiments.

With the above setup, the CFD model has been run monitoring the average glass temperature and the heat losses towards the external ambient. The comparison of the results (see Table 8) shows a good agreement between the numerical results and the experimental data. The deviation in the computed heat losses is always lower than 1%, while the relative error in the glass temperature (considering the temperature jump with respect to the ambient) is  $\approx 4\%$  and  $10\%$ , when the absorber tube temperature is 521.85 K and 567.85 K respectively. Although the relative error in the glass temperature is not completely negligible, especially in the second case ( $T_{abs} = 567.85$  K), the absolute error is really small, being always lower than 3 K.

Table 8 – Comparison between experimental data and computed results from 2D thermal model in terms of glass temperature ( $T_g$ ) and heat losses ( $q'_{loss}$ ) at given absorber temperature ( $T_{abs}$ )

	$T_{abs}$ [K]	$T_g$ [K]	$q'_{loss}$ [W/m]
Experiment	521.85	315.15	70.2
CFD	521.85	314.40	70.4
Experiment	567.85	324.25	107.3
CFD	567.85	321.30	108.3

### 5.1.2 Case of wind across the collector

In the case of wind direction normal to the absorber tube axis, the 2D CFD model described above can still be used, with the only differences regarding:

- The dimensions of the external air region. The external air domain has been stretched along the wind direction in order to fully describe the velocity field around the receiver unit, including in the computational domain also the vortex released downstream the receiver. The resulting shape is rectangle 4 m high and 10 m width (see Figure 15).
- The boundary conditions applied to the external region: on the top, bottom and downwind borders the pressure outlet boundary condition has been applied, imposing ambient pressure. The wind inlet side has been modeled imposing a uniformly distributed wind velocity, set equal to the reference value of 3.7 m/s (see Table 3), and assuming the wind direction normal to the border, see Figure 15. Regarding the air temperature, it has been set equal to the ambient value; see Table 3.

The grid has been generated in this case keeping the same average size of the cells around the receiver as in the case without wind, resulting in  $\sim 9.5 \times 10^4$  cells.

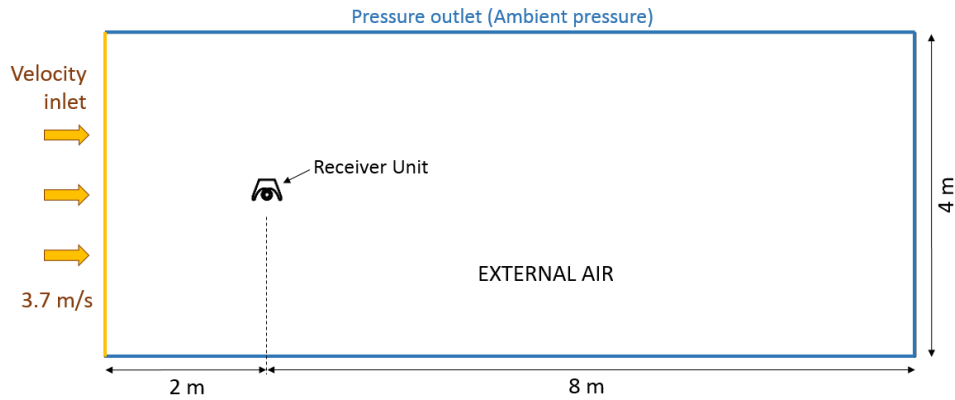


Figure 15 – Computational domain and boundary conditions for the 2D model in the wind across case

An example of the computed external air velocity field is shown in Figure 16 only for the simply-encapsulated configuration since no remarkable differences can be detected in the evacuated case, similarly to what was observed in the windless case. Moreover, in the presence of wind the glass surface temperature affects the external air motion less than in the absence of wind, since this motion is not driven by natural convection anymore. As expected, vortices appear downstream of the receiver unit - they are practically extinguished at the end of the considered domain. Figure 16 also suggests that the CPC unit shields the receiver tube from the external air flow. In fact, the region under the secondary concentrator is characterized by a relatively low air speed. As a consequence of the CPC shielding effect, the convective heat losses is not expected to dramatically increase due the presence of the wind

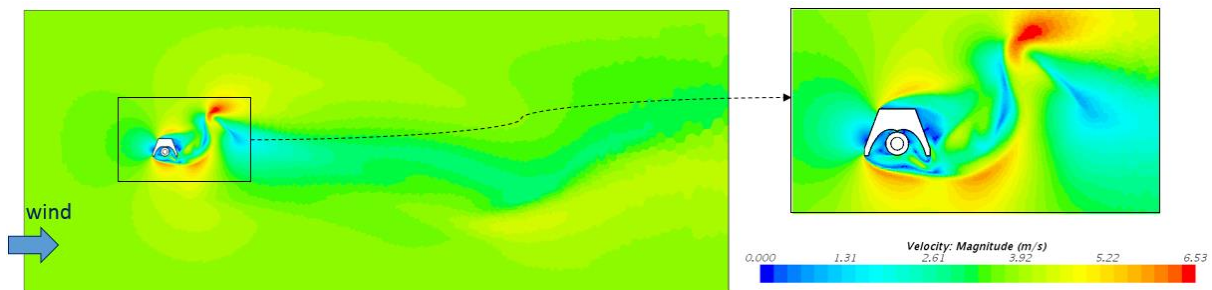


Figure 16 – Computed velocity magnitude contours around the receiver unit (case of wind across the receiver), assuming  $T_{oil} = 513$  K: simply-encapsulated tube.

Figure 17 shows the temperature field around the receiver unit for the two configurations analyzed here. The comparison with the contours in the absence of wind (Figure 14) shows a similar temperature field, especially in the

gap region for the simply-encapsulated configuration. The main difference with the no-wind case can be detected in the bottom part of the receiver unit, where a stream of hot air leaves the region under the secondary concentrator, due to the wind. This causes a reduction of the air temperature around the glass envelope (promoting the convective losses), since the hot air leaving this region is replaced with fresh air at ambient temperature.

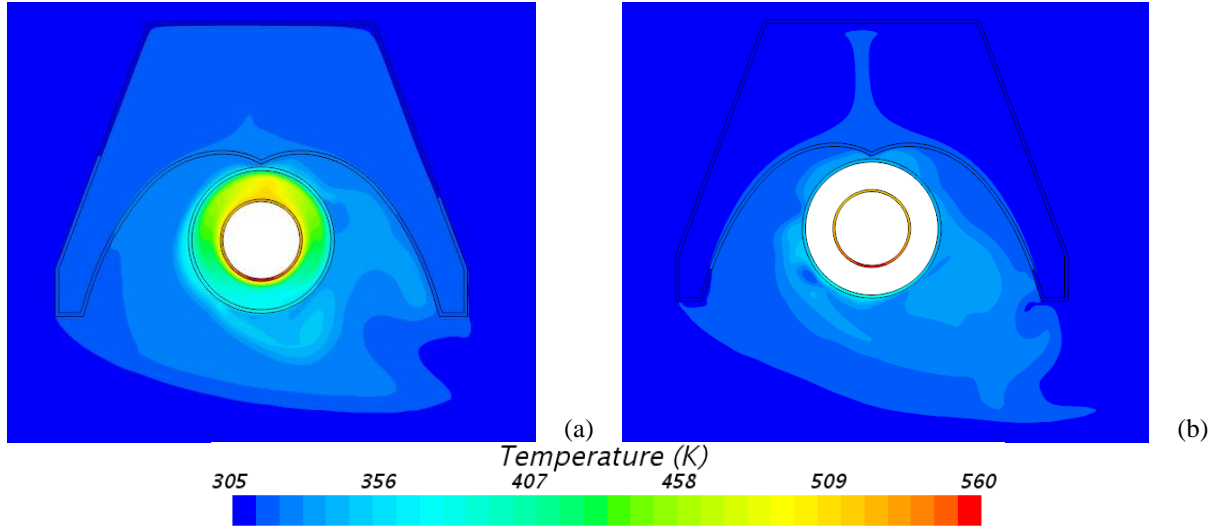


Figure 17 – Temperature field computed around the receiver unit (case of wind across the receiver), assuming  $T_{oil} = 513$  K: (a) simply encapsulated tube, (b) evacuated tube, respectively.

### 5.1.3 Receiver performance

The performance of the two receiver configurations has been evaluated both in the absence of wind and in the case of wind across the collector axis.

Starting with the no-wind case, it is shown in Figure 18 that the evacuated tube performs better than the simply encapsulated one, as expected: the total heat losses are always less than half of the non-evacuated case.

The difference between the two configurations can be easily identified in the convective share of the heat losses, which is absolutely negligible in the case of the evacuated tube, see Figure 19. On the contrary, the radiative heat loss is comparable, since the temperature of the absorber tube is practically the same (it depends mainly on the oil temperature) and the temperature of the glass cover changes modestly.

Starting from the output data of the CFD analysis, a quadratic best fit has been computed to obtain a correlation between the overall heat losses and the difference  $\Delta T$  between the oil and the environment temperature (see Figure 18). The useful heat flux transferred to the working fluid has been also evaluated, deriving a correlation between the thermal power transferred to the fluid and the difference between the oil and the environment. This correlation is finally exploited to drive the 1D thermal model, see Figure 3.

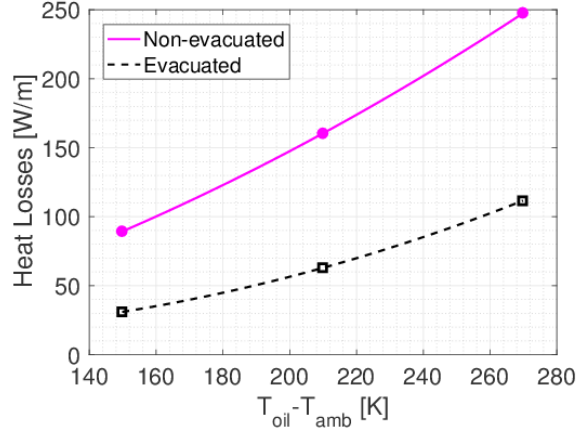


Figure 18 – Fit of the computed total (convective + radiative) heat losses from the absorber tube in the absence of wind as a function of the difference between the oil temperature and the ambient temperature. The results for both evacuated (dashed line) and non-evacuated (solid line) tube are reported.

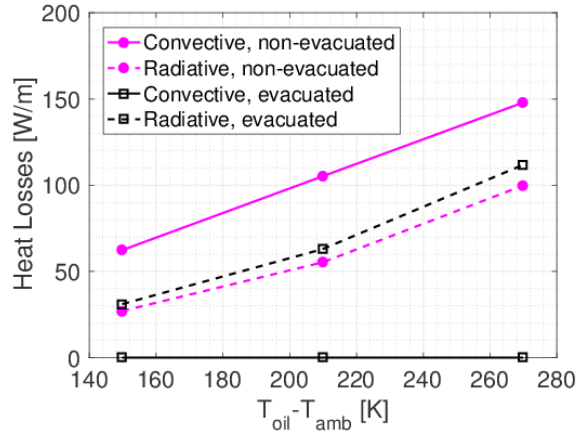


Figure 19 – Computed convective (solid lines) and radiative (dashed lines) heat losses from the absorber tube in the absence of wind for the evacuated (open squares) and non-evacuated (solid circles) tube, respectively.

The receiver efficiency, according to Eq. 2, can be defined as

$$\eta = q'_{fluid} / q'_{abs} \quad (6)$$

Despite the different thermal behavior in terms of heat losses, the receiver efficiency is considerably high in both configurations; see Figure 20. This is because the heat losses are in any case a very small share of the heat absorbed by the absorber tube.

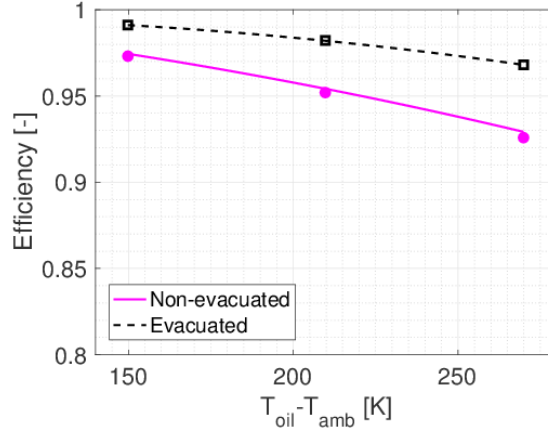


Figure 20 – Receiver efficiency computed in the absence of wind as a function of the difference between the oil temperature and the ambient temperature for the evacuated (dashed line) and non-evacuated (solid line) tube, respectively.

The same procedure described in the no-wind case has been applied in case of wind across the receiver to determine the heat losses from the absorber tube and the useful heat transferred to the working fluid as a function of the difference between the oil and the environment temperature.

Figure 21 provides a comparison between the overall heat losses from the absorber tube in the presence of wind (across the receiver) and in the absence of wind.

The simply encapsulated configuration is clearly affected by the presence of wind: the increase in the overall heat losses ranges between 37% (@ 453 K) and 72% (@ 573 K). However, the heat losses are still a very small share of the power absorbed by the absorber tube; hence, the wind effect on the receiver performance is quite modest (the efficiency decreases from 97.4% to 95.9% and from 92.6% to 90.7% @ 453 and 573 K respectively). On the other hand, no significant changes occur in the evacuated case. This is because the glass cover in the simply encapsulated configuration is less thermally decoupled from the absorber tube with respect to the evacuated configuration, which takes advantages from the insulation effect provided by the vacuum in the gap.

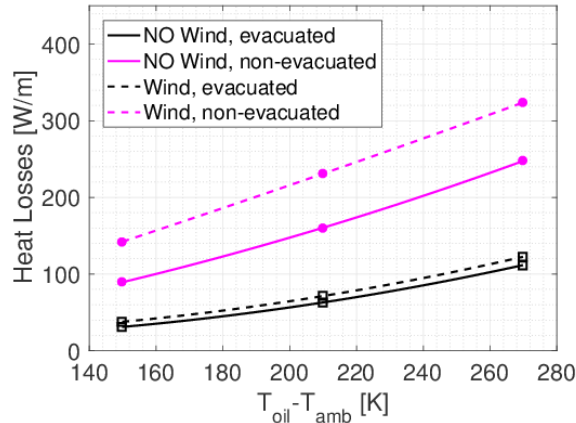


Figure 21 – Overall heat losses computed from the absorber tube for the evacuated (open squares) and non-evacuated (solid circles) configurations: comparison between the case in the absence of wind and the case of wind (solid lines) across the receiver (dashed lines).

#### 5.1.4 Comparison with a lumped-parameter model based on correlations

To prove the reliability of the results obtained above from the 2D thermal model, they have been compared with the ones obtained from the available correlations. This comparison can in turn provide useful information about the accuracy of the existing correlations in this kind of problems, where a not common and quite complex receiver shape, which also includes the secondary concentrator, has to be analyzed. For this purpose, a lumped-parameter model has been built, based on the one developed in (Forristall, 2003) that describes the steady-state thermal behavior of a linear

receiver for parabolic trough systems. The heat transfer phenomena considered in the model are identified in Figure 22a, while Figure 22b shows the equivalent thermal resistance scheme.

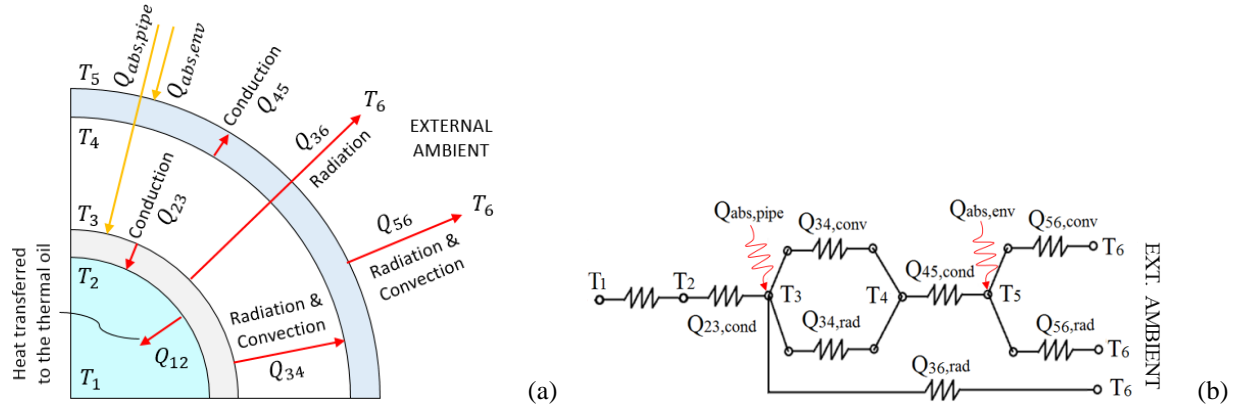


Figure 22 – Lumped-parameter 1D model: (a) heat fluxes along the radial direction; (b) electrical network analogy.

With respect to the model developed by Forristall, the following assumptions have been made:

- The heat loss by conduction through the support structures has been neglected, according to (Österholm and Pålsson, 2014).
- To calculate the heat loss by radiation from the glass envelope to the external structure, the ambient temperature has been considered instead of the colder sky temperature. In fact, the glass cover does not see the sky above it, but the CPC surface, that is slightly hotter than the ambient temperature.
- The assumption made by Forristall of completely opaque glass envelope has been removed. The transmissivity of the glass at the thermal radiation has been set equal to 0.11, as discussed in section 5.1.1, in order to make the lumped-parameter model as much as possible coherent with the CFD model.

The heat transfer between the absorber tube and the glass cover occurs both by convection and by radiation. The latter ( $Q_{34,rad}$ ) is given by Eq. 7.

$$Q_{34,rad}[W/m] = (1 - \tau) \frac{\sigma \pi D_3 (T_3^4 - T_4^4)}{1/\varepsilon_3 + (1 - \varepsilon_4) D_3 / (\varepsilon_4 D_4)} \quad (7)$$

where  $\sigma$  is the Stephan-Boltzmann constant,  $T_4$  is the temperature of the inner glass tube surface,  $D_4$  is the inner diameter of the glass cover,  $\varepsilon_3$  is the emissivity of the selective coating applied on the absorber tube surface, while  $\varepsilon_4$  is the glass envelope emissivity. Finally, the term  $\tau$  indicates the transmissivity of the glass envelope to the infrared thermal radiation. On the other hand, the convective heat flux  $Q_{34,conv}$  is calculated on the base of the receiver typology.

In the case of a simply encapsulated receiver, we refer to Eq. 8.

$$Q_{34,conv}[W/m] = \frac{2.425 k_{34} (T_3 - T_4) (Pr Ra / (0.861 + Pr))^{1/4}}{(1 + (D_3/D_4)^{3/5})^{5/4}} \quad (8)$$

where  $k_{34}$  is the air thermal conductivity in the gap at the mean temperature between  $T_3$  and  $T_4$ .  $Pr$  and  $Ra$  indicate the Prandtl and Rayleigh numbers, respectively, which are evaluated always at the mean temperature between  $T_3$  and  $T_4$ . The characteristic length adopted to calculate the Rayleigh number is the outer diameter of the absorber ( $D_3$ ).

In the case of an evacuated receiver tube, we refer to Eq. 9.

$$Q_{34,conv}[W/m] = \pi D_3 h_{34} (T_3 - T_4) \quad (9)$$

where  $h_{34}$  represents the convective heat transfer coefficient in case of air at very low pressure (vacuum conditions). A proper value proposed in the literature is  $1.115 \times 10^{-4} \text{ W/m}^2\text{K}$  (Forristall, 2003).

The absorber tube also dissipates heat by radiation directly towards the external ambient, being the glass of the cover partially transparent to the thermal radiation. This quantity ( $Q_{36,rad}$ ) has been evaluated as in Eq. 10.

$$Q_{36,rad}[W/m] = \tau \cdot \sigma \varepsilon_3 \pi D_3 (T_3^4 - T_6^4) \quad (10)$$

where  $T_3$  is the outer absorber tube temperature and  $T_6$  is the ambient temperature in reference conditions (see Table 3). Regarding the heat transfer between the outer surface of the glass envelope and the external ambient, both radiative and convective losses occur. The radiative term has been evaluated using Eq. 11.

$$Q_{56,rad}[W/m] = \sigma \varepsilon_4 \pi D_5 (T_5^4 - T_6^4) \quad (11)$$

while the convective heat flux has been computed as shown in Eq. 12.

$$Q_{56,conv}[W/m] = \pi D_5 h_5 (T_5 - T_6) \quad (12)$$

In Eqs. 11 and 12,  $D_5$  is the outer glass tube diameter and  $h_5$  is the convective heat transfer coefficient. The latter has been evaluated as a function of the Nusselt Number, which in turn has been calculated depending on the dominant convection phenomena (natural or forced).

According to (Forristall, 2003), the correlation developed by Churchill and Chu (Incropera et al., 2012) is used in the absence of wind (natural convection), while the Zukauskas's correlation (Incropera et al., 2012) has been applied in the case of wind across the collector (forced convection). Both these correlations were developed considering cylindrical tubes at uniform temperature.

The outcomes of the lumped-parameter model and of the CFD analysis have been compared in terms of heat losses from the absorber tube. Starting from the no wind case, Figure 23 shows that a good match is obtained between the outcomes of the CFD model and those of the lumped-parameter model for the evacuated configuration, while in the case of the simply-encapsulated configuration, the lumped-parameter model tends to overestimate the overall heat losses. This is due to the convective share of the overall heat losses (which is absolutely negligible in the evacuated case) that is strongly overestimated by the correlations, see Figure 24a. In fact, the CFD model takes into account also the effect of the CPC unit that allows keeping a relatively high temperature of the external air around the glass envelope, which in turn determine a higher temperature of the glass cover at equal absorber tube temperature. Imposing the same glass temperature, the difference between the convective heat losses evaluated by the two models is strongly reduced. Regarding the radiative heat losses, the outcomes of the lumped parameter model are almost the same of the CFD one, see Figure 24b. The radiative heat losses evaluated by means of the lumped parameter model are just slightly overestimated due to the lower glass cover temperature.

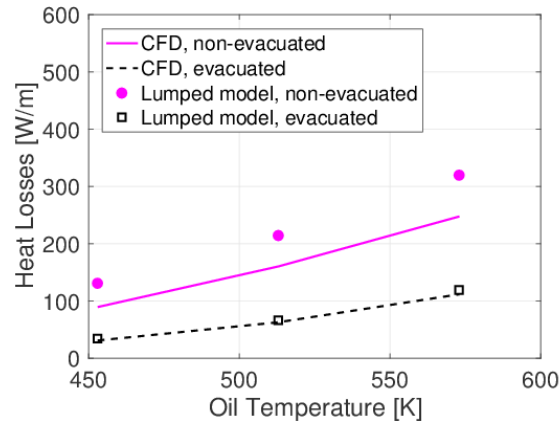


Figure 23 – Heat losses (convective + radiative) from the absorber tube calculated with the CFD (lines) and 1D lumped approaches (symbols), for the evacuated and non-evacuated receiver configurations, respectively, in the absence of wind.

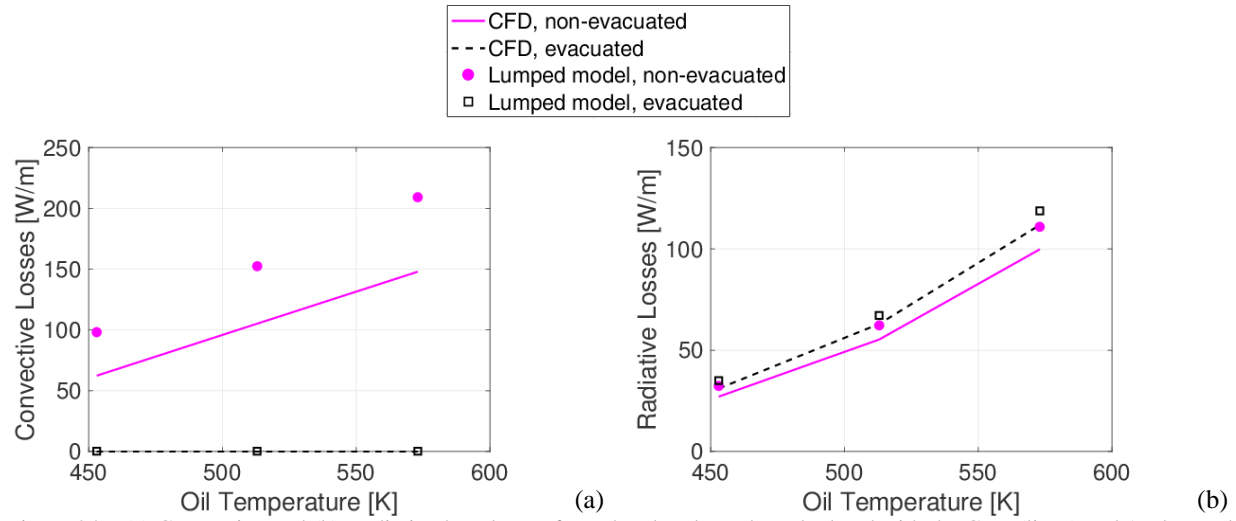


Figure 24 – (a) Convective and (b) Radiative heat losses from the absorber tube calculated with the CFD (lines) and 1D lumped approaches (symbols), for the evacuated and non-evacuated receiver configurations, respectively, in the absence of wind.

Moving to the case where the presence of the wind across the receiver is considered, the comparison between the CFD and the lumped-parameter model provides the same results of the no wind case. In fact, looking at Figure 25, a good agreement is obtained for the evacuated configuration, where the convective heat flux from the absorber tube to the glass envelope is negligible, while in the simply-encapsulated configuration the overall heat losses are overestimated by the correlations due to the lower glass temperature calculated by the lumped parameter model. In this case, the higher glass temperature evaluated in the CFD model is linked with the shielding effect of the CPC unit that protects the glass envelope against the direct external air flow.

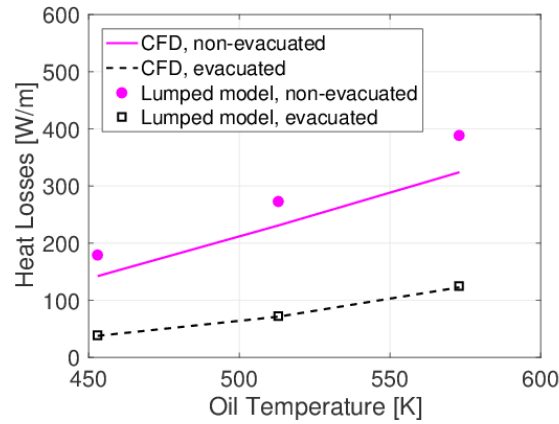


Figure 25 – Heat losses (convective + radiative) from the absorber tube calculated with the CFD and 1D lumped approaches, for the evacuated and non-evacuated receiver configurations, respectively, in the case of wind across the receiver.

### 5.1.5 Sensitivity analysis: coating emissivity

According to what has been discussed up to now, the thermal efficiency of the receiver analyzed here is quite high in both the evacuated and the simply encapsulated configurations. The selective coating (CERMET) applied on the receiver tube plays a key role in obtaining high thermal performance, since it ensures a very low surface emissivity,  $\sim 0.09$  in the range of temperatures of interest, that in turn limits the radiative heat losses.

Therefore, an interesting point is to evaluate how the receiver performance changes if a less performing coating is adopted. In particular, a non-selective coating is considered, the Pyromark 2500 (Ho et al., 2013), whose average surface emissivity is about 0.84 in the temperature range of this application. This sensitivity analysis has been conducted for the evacuated and the simply encapsulated tube in the case of wind blowing across the receiver axis; the results are shown in Figure 26.

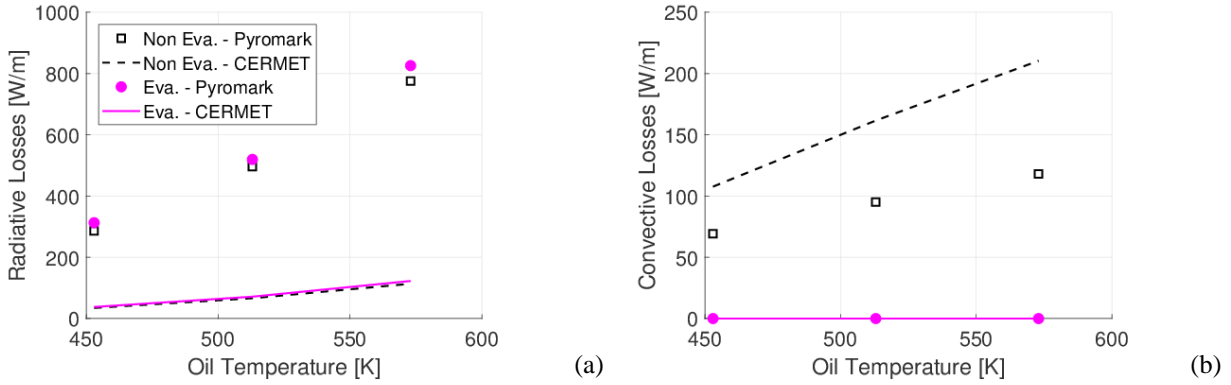


Figure 26 – (a) Radiative and (b) convective heat losses for an evacuated and simply encapsulated absorber tube in the case of wind blowing across the receiver axis; comparison between CERMET (lines) and Pyromark (symbols)

According to Figure 26, the radiative heat losses strongly increase using a non-selective coating, as expected. The increase is in the range of 6.7-8.3 times depending on the oil temperature and it is practically the same for the evacuated and simply encapsulated configuration since the different emissivity affects the radiative losses, which are not directly influenced by the thermal insulation provided by the vacuum in the gap.

The higher radiative heat flux that leaves the absorber tube leads to an increase of the glass cover temperature and consequently of the temperature of the air in the gap (simply encapsulated configuration). For this reason, the convective share of the heat losses is reduced when a non-selective coating is applied, as shown in Figure 26b.

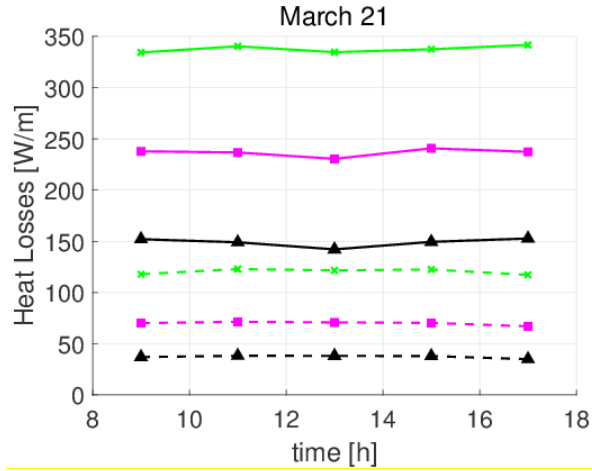
#### 5.1.6 Receiver performance at different DNI and sun position

In this section, the impact of the DNI level and of the sun position on the receiver performance is assessed considering different days along the year and different hours within the day starting from the data reported in (Soltigua 2015); in particular, the same days and times already explored in section 4.1 are taken into account here.

This study has been conducted only in the case of wind blowing across the receiver axis to maintain the computational cost within a reasonable time. The wind-across case has been selected instead of the case in the absence of wind because it allows observing larger differences in the thermal performance of the evacuated and simply encapsulated tubes. The ambient temperature is imposed equal to the reference value (see Table 3), while the inner heat transfer coefficient between the absorber tube and the oil flow is calculated according to Eq. 4, assuming a mass flow rate equal to 2.2 kg/s.

The results of this analysis highlight that the heat losses are almost constant during the day for a given oil temperature (see Figure 27); hence, they are practically not influenced by the solar load, as observed also in (Qiu et al., 2015). This is because the heat losses depend on the absorber tube temperature, which does not change significantly with the DNI level since it is strongly linked to the imposed oil temperature. In fact, thanks to the quite high internal convective heat transfer coefficient ( $>750 \text{ W/m}^2\text{K}$  in any case), the absorbed heat is transferred to the oil flow by means of a relatively small temperature gradient between the oil and the tube wall. For the same reason, no remarkable differences can be observed among the different simulated days; hence, only the results obtained for March 21 are shown in Figure 27.

Figure 27 indicates that the heat losses, which increase with the oil temperature, are always higher in the case of the simply encapsulated tube, independently of the oil temperature.



—▲— Non Evac. 453 K —▲— Evac. 453 K —■— Non Evac. 513 K —■— Evac. 513 K —x— Non Evac. 573 K —x— Evac. 573 K

Figure 27 – Heat losses (convective + radiative) from the absorber tube calculated using the CFD 2D model for both the evacuated (dashed lines) and non-evacuated (solid lines) configurations at different oil temperatures (453, 513 and 573 K) for March 21.

Although the heat losses are more or less the same for a given oil temperature, the solar heat absorbed by the absorber tube changes on the base of the DNI level and of the sun position, since that affects the optical efficiency (see Figure 9). This means that the thermal efficiency changes in a non-negligible way during the day, being higher where the heat absorbed is higher. Figure 28 shows that the thermal efficiency decreases moving away from the noon, due to the lower absorbed heat. However, the reduction of the thermal efficiency is more remarkable in the case of the simply encapsulated tube, while the evacuated configuration suffers less the changes in the absorbed power. This is because the evacuated tube benefits from the thermal insulation provided by the vacuum in the gap that leads to very low heat losses, as visible in Figure 27, which represent a modest share of the absorbed heat also far from the solar noon.

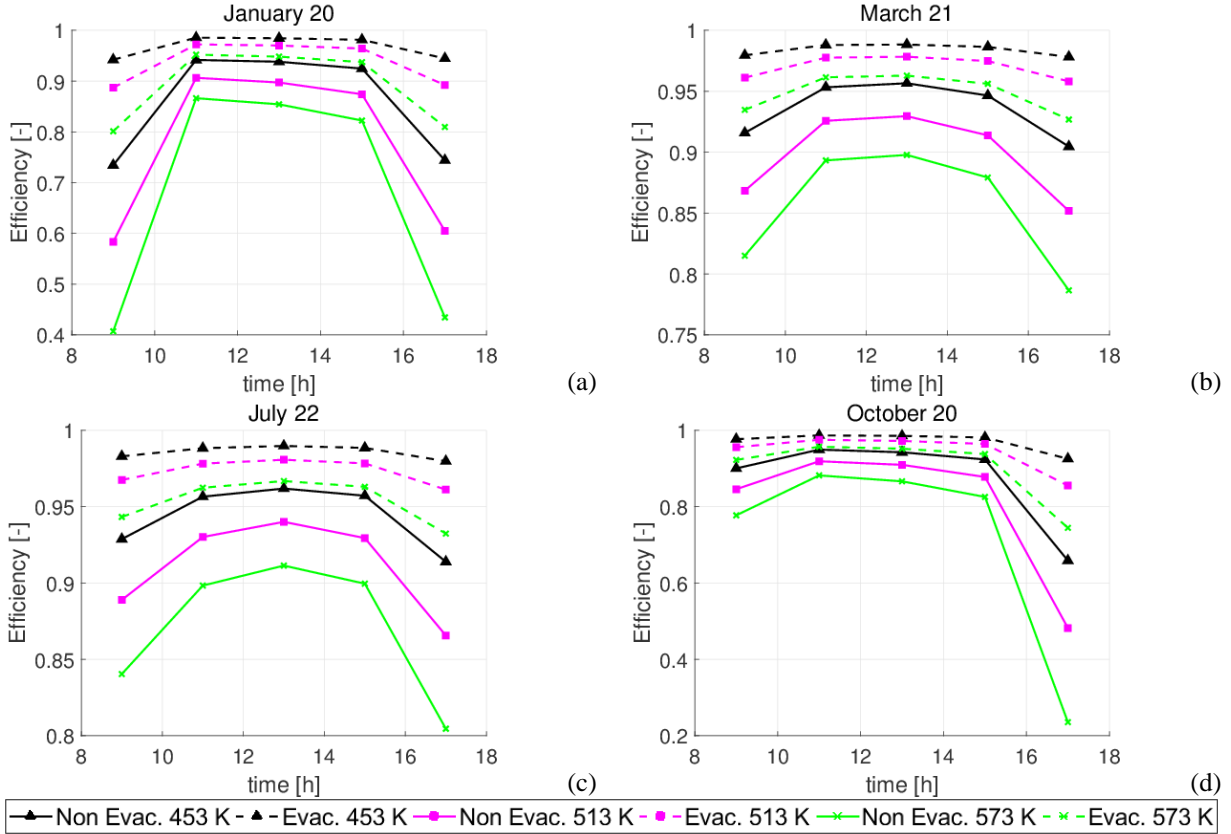


Figure 28 – Thermal efficiency calculated using the CFD 2D model for both the evacuated (dashed lines) and non-evacuated (solid lines) configurations at different oil temperatures (453, 513 and 573 K) considering different days and hours

The results from this annual analysis can be exploited to calculate an approximate value of the annual efficiency that provides a first measure of the benefit given by an evacuated tube. The integral value of the annual thermal efficiency is determined assuming that each day considered here is representative for the corresponding season and that each hour simulated is representative of an equal time interval within the day. Therefore, the arithmetic average among the considered points has been calculated, which is equal to  $\sim 0.85$  in the case of the simply encapsulated tube and  $\sim 0.95$  for the evacuated one; this means that the thermal efficiency increase due to the use of an evacuated tube is about 10%.

## 5.2 3D CFD model

The 3D steady-state thermal model has been developed with the aim of analyzing the case in which the wind direction is parallel to the receiver axis, which cannot be handled with a 2D model. This situation is particularly important for the reference plant analyzed in this paper. In fact, the dominant wind direction in the plant site is North-South, like the solar field; hence, the wind will most likely flow along the receiver axis, and the study of its effect is particularly important to evaluate the performance of the linear receiver.

The aim of the 3D model is to determine the percentage of heat losses increase due to an external air stream blowing along the collector with respect to the no-wind case. The wind effect on the heat losses is expected to decrease moving downstream from the leading edge and to reach an asymptotic value, due to the development of the boundary layer which will then bring the flow to an almost fully developed condition, this problem being a sort of mixture between internal and external flow. For this reason, it will be sufficient to simulate just a small portion of the entire length of the hydraulic loop.

The computational domain of the 3D model is obtained extruding the 2D cross section model along the receiver axis, as shown in Figure 29. The extruded length is equal to 16 m. However, some simplifications with respect to the 2D model have been made, in order to keep the computational cost within acceptable limits:

- The air volume inside the CPC unit (see Figure 10) has not been included in the computational domain.
- The imposed heat flux on the absorber outer surface has been replaced as boundary condition by the temperature distribution computed along the axis post-processing the results of the 2D and 1D models in the absence of wind (Figure 31). This simplification is justified by the fact that the temperature profile along the tube does not change significantly in case of wind due to the modest increase of the heat losses (see below). Consequently, the thickness of the absorber tube and the heat transferred to the working fluid have not been considered in the simulation.

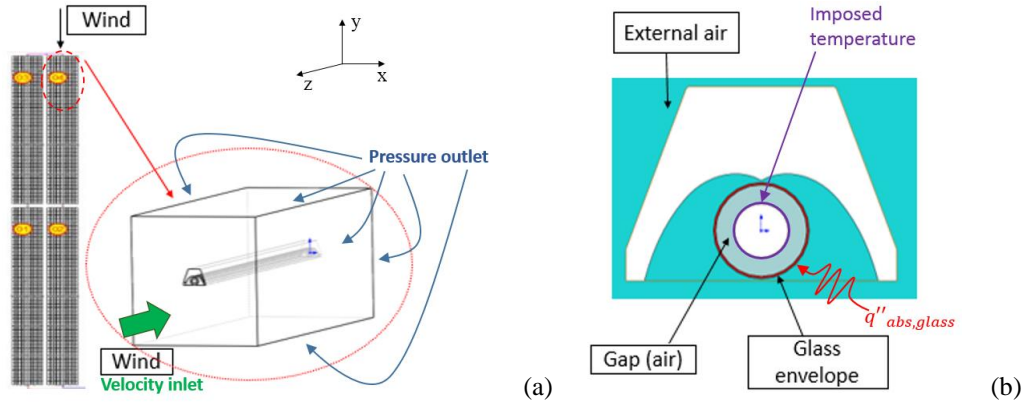


Figure 29 – 3D model: simulated regions, boundary conditions and thermal drivers: (a) on the external air region and (b) on the receiver unit.

As shown in Figure 29, only the receiver module first hit by the wind flow is considered in the model. The same figure provides a sketch of the simulated regions, thermal drivers and boundary conditions. At the collector ends there are no vertical plates that prevent the wind from entering in the cavity under the CPC. The mesh generated for the 3D model (see Figure 30) has of about 3 millions of cells. The mesh base size in the refined area below the CPC has been set equal to 5 mm, which is larger with respect to the 2D case ( $\approx 2$  mm, see Figure 11) in order to keep an acceptable computational time. A convergence analysis has been performed (not shown) to check the grid independence of the results.

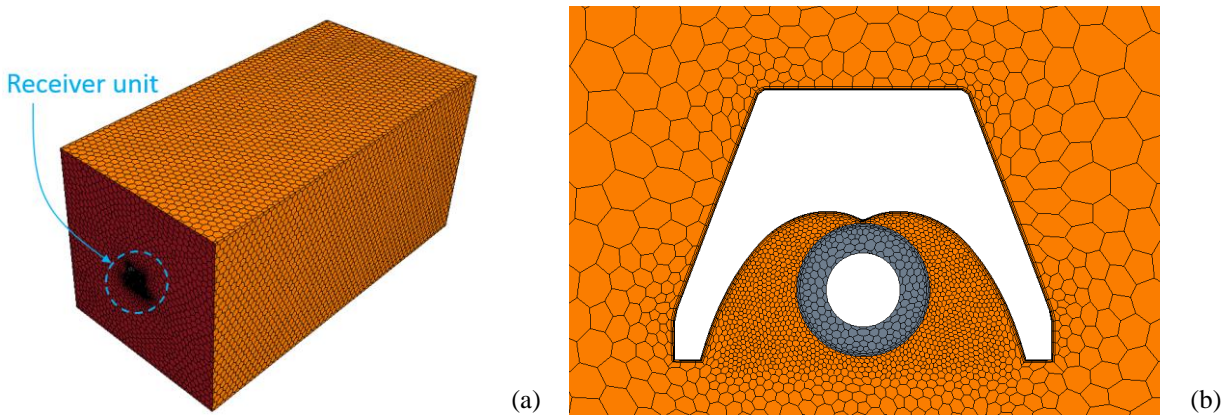


Figure 30 – (a) Mesh generated for the 3D model; (b) zoom on the receiver.

All the borders of the external air domain have been set as pressure outlet, imposing the ambient pressure defined in Table 3, with the exception of the wind inlet side, where the velocity inlet boundary condition has been applied, imposing a wind speed equal to 3.7 m/s. The solar field is oriented at  $17.5^\circ$  from the North-South, while the wind flows exactly along the North-South direction. In the model, it is assumed that the wind blows perfectly parallel to the receiver axis.

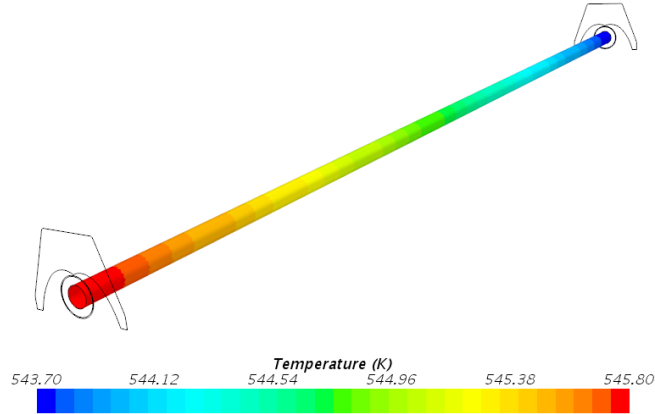


Figure 31 – 3D model: thermal driver applied on the outer wall of the absorber tube: axial temperature distribution for a specific portion of the linear receiver evaluated post-processing the 2D model results.

The 3D model has been run first in the absence of wind (all the boundary conditions applied on the borders of the external air domain have been replaced with the so-called “stagnation inlet”) in order to:

- Evaluate if the computed heat losses matched with the ones computed post-processing the output of the 2D model
- Provide a baseline to determine the heat losses increase due to the wind.

The computed results indicate that the deviation in the overall heat losses between the 3D and 2D models is about 3% for the evacuated configuration, while for the simply encapsulated one the deviation is about 7% due to the simplifications adopted in the 3D model.

In Figure 32, an example of the computed axial velocity field on different cross sections along the receiver axis is displayed. It is shown that the boundary layer under the CPC unit tends to develop like in a close pipe moving away from the leading edge. Of course, in the region under the receiver tube the boundary layer cannot be confined by the CPC unit, i.e. it will continue to grow up to surface of the mirrors. As expected, Figure 32 shows that the air speed around the receiver tube slows down moving away from the leading edge (wind inlet).

The development of the air flow under the CPC can be also observed in Figure 33, which shows the velocity profiles on a horizontal plane passing through the receiver axis at different locations along the receiver length.

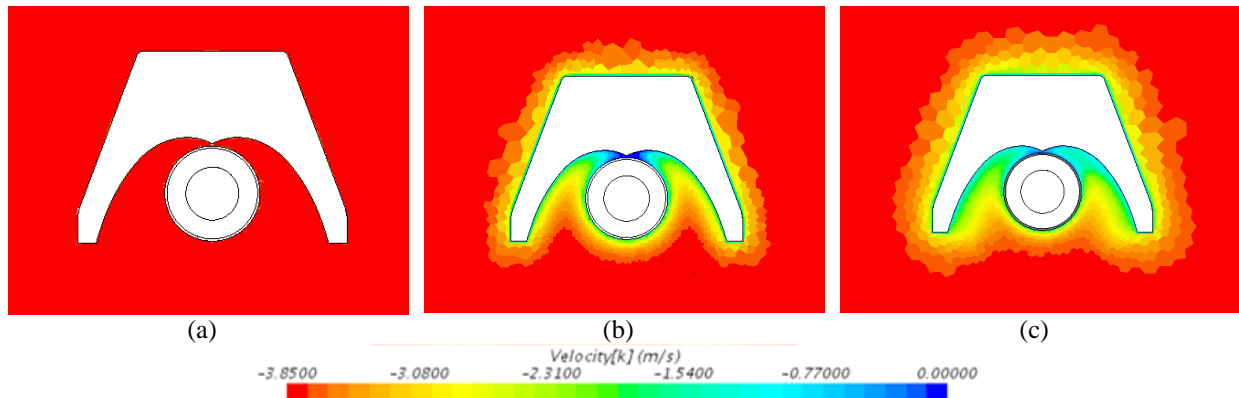


Figure 32 – Contours of the z-component of the air velocity on the xy plane for the evacuated configuration, at (a) wind inlet ( $z = 0$  m), (b)  $z = 2$  m and (c)  $z = 4$  m.

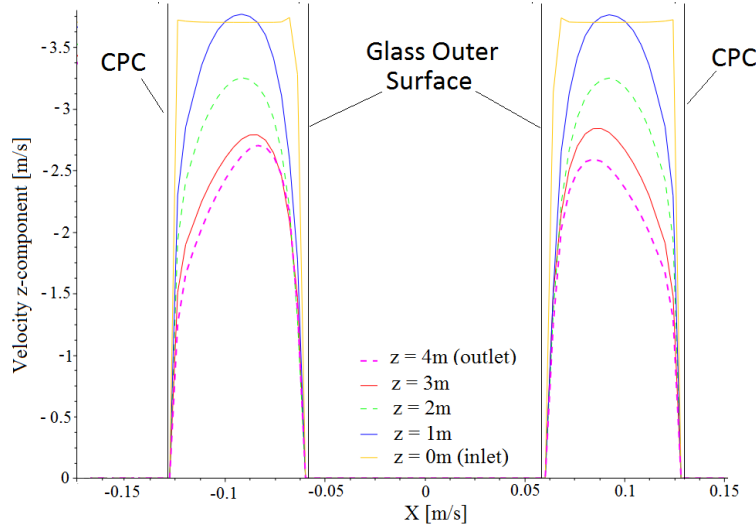


Figure 33 – Velocity profile (z-component) on a horizontal plane through the receiver axis at different locations from the leading edge (evacuated configuration).

The goal of the 3D model is to determine the heat losses from the absorber tube in the case of wind blowing along the collector. The results of this analysis are provided in Figure 34 for the simply encapsulated tube and in Figure 35 for the encapsulated configuration.

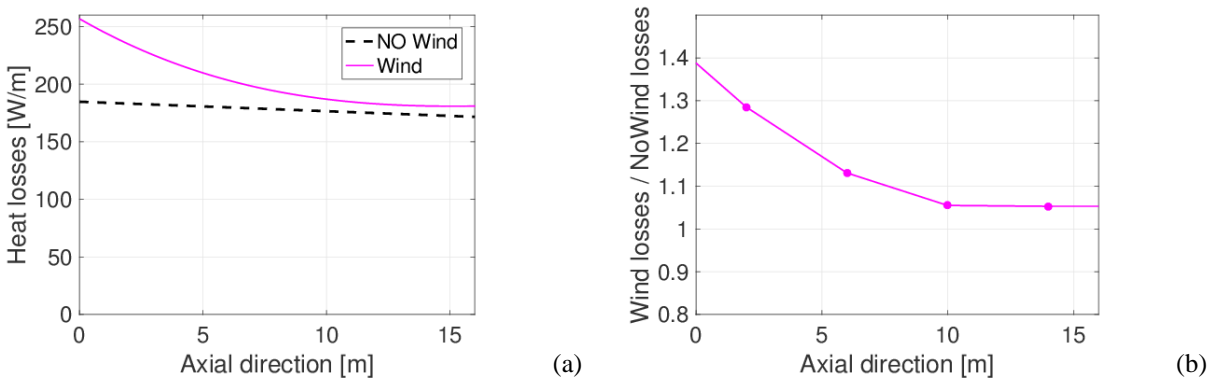


Figure 34 – Simply encapsulated tube: (a) Computed heat losses (from the absorber tube) in case of wind blowing along the receiver axis for the first 16 m of receiver length starting from the leading edge (solid line) and in the absence of wind (dashed line); (b) percentage of increase of the losses in case of wind along the receiver with respect to the case in the absence of wind.

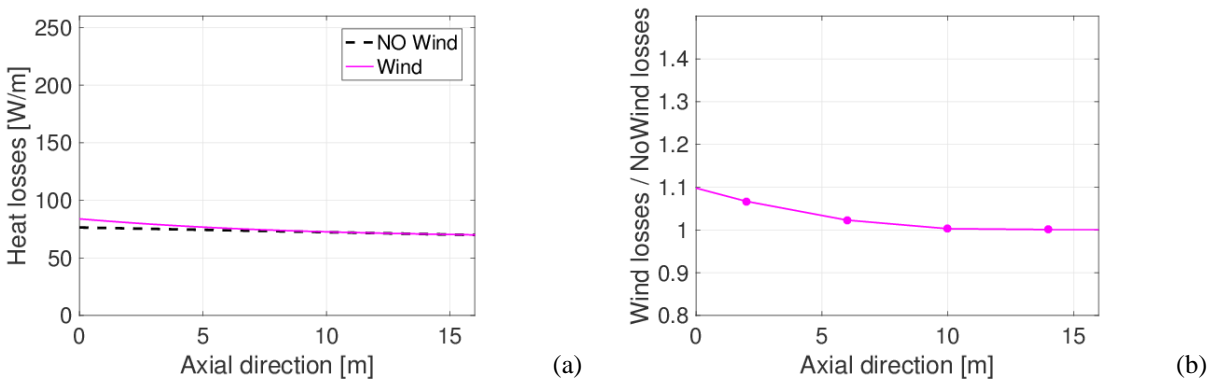


Figure 35 – Evacuated tube: (a) Computed heat losses (from the absorber tube) in case of wind blowing along the receiver axis for the first 16 m of receiver length starting from the leading edge (solid line) and in the absence of wind (dashed line); and (b) percentage of increase of the losses in case of wind along the receiver with respect to the case in the absence of wind.

According to Figure 34, in the case of a simply encapsulated tube, after about 14 m from the leading edge the heat losses can be considered independent from the receiver axis coordinate. In this zone, the presence of the wind increases the heat losses by about 5.3%, while at the wind inlet section this percentage approaches 40%. Thus, most of the collector length ( $\approx 90\%$ ) is not dramatically affected by the wind. The evacuated tube (Figure 35) is even less affected by the external air flow (negligible heat losses increase after 10 m), as already observed in case of wind across the receiver axis, see Figure 21 and the discussion thereof.

Results from the 3D analysis have been used to correct the heat losses evaluated by means of the 2D model in the no-wind case, as shown in Eq. 13.

$$q'_{loss,windAlong} = \beta \cdot q'_{loss,noWind} \quad (13)$$

where  $q'_{loss,windAlong}$  corresponds to the heat losses, in W/m, from the absorber tube in the case of wind along the collector,  $q'_{loss,noWind}$  are the heat losses evaluated thanks to the 2D model in absence of wind (see Figure 18), and  $\beta$  is the correction factor determined from the 3D analysis as a function of the axial position, see Figure 34b and Figure 35b.

The heat transferred to the working fluid has been then computed (see Eq. 2) and finally exploited in the 1D model to simulate the entire loop also in the case of wind along the collector axis.

## 6 Analysis of the collector performance

The receiver thermal behavior has been analyzed along the entire length of a hydraulic loop by means of the 1D thermal model described in section 3. A very small number of elements ( $\sim 10$ ) is required to simulate the whole hydraulic loop (270 m) ensuring the grid independence of the solution. The results are evaluated in terms of oil temperature distribution along the receiver axis for both the receiver configurations considered in the present study, in the case of the absence of wind, wind blowing across the collector and wind blowing along the collector. In the first two conditions, the 1D model is directly driven by the results of the 2D CFD analysis. The third case has been simulated increasing the heat losses computed in the absence of wind with the detailed 2D model by the percentage estimated in section 5.1.5 using the 3D model, see Eq. 13. Then, the useful heat transferred to the working fluid has been calculated according to Eq. 2. The computed oil temperature profile along the hydraulic loop is shown in Figure 36 for the no-wind case; considering the presence of wind (across or along) the temperature profile along the receiver axis does not change significantly (not shown). In fact, as observed in the previous sections, the presence of the wind practically does not affect the thermal behavior of the evacuated configuration, while it reduces modestly the receiver performance of the simply encapsulated configuration (the heat losses are a small share of the heat flux absorbed by the absorber tube also in the presence of wind). As already observed, this modest impact of the wind on the performance is mainly due to the shielding effect of the CPC unit, which protects the receiver tube from the external air flow.

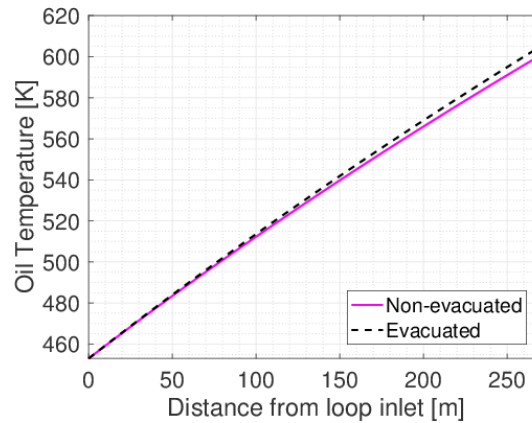
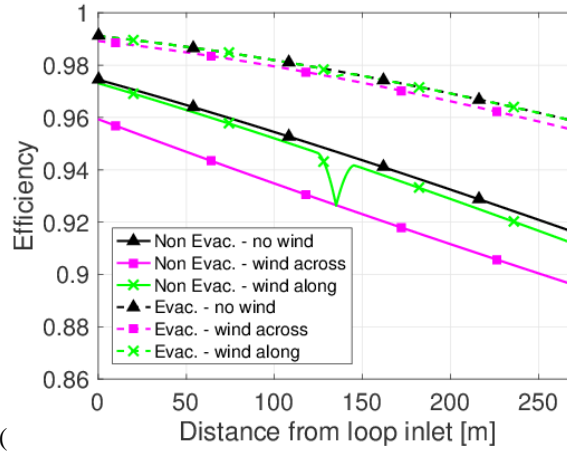


Figure 36 – Thermal oil temperature evolution along the receiver tube in the absence of wind, for the simply encapsulated (solid line) and evacuated (dashed line) tube, respectively.

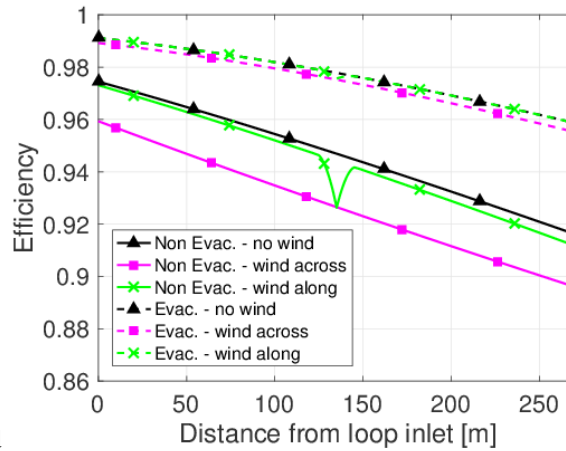
Comparing the oil temperature profiles for the simply encapsulated and evacuated tube in Figure 36, no remarkable differences can be observed between the two configurations, as expected on the base of what has been discussed above. Moreover, Figure 36 indicates that both the analyzed receiver configurations lead to an oil outlet temperature higher than the desired operational value (573 K). In order to obtain the desired temperature at the outlet section, one could think of increasing the oil mass flow rate in the absorber tube.

Knowing the oil temperature profile along the receiver length, the corresponding local heat losses (Figure 37) and the



thermal efficiency (

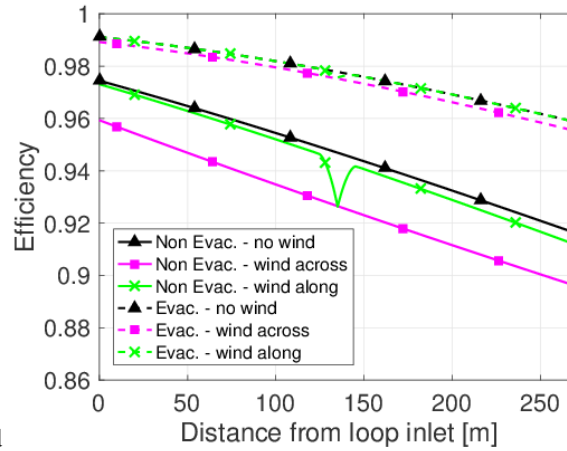
Figure 38) can be also evaluated, on the base of the correlations determined thanks to the CFD analysis. These quantities have been evaluated for both the receiver configurations studied and for all the wind conditions examined.



Looking at Figure 37 and

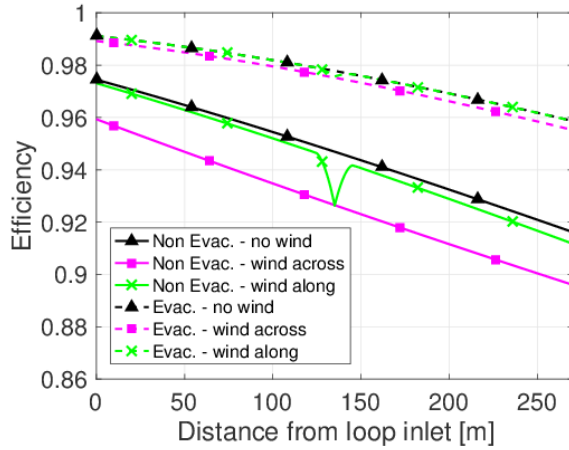
Figure 38 (simply encapsulated tube), in the case of wind along the receiver, the peak in the heat losses and efficiency trends is due to the wind that impacts on the collector structure at the summit of the “U-shape” of the hydraulic loop (see Figure 29). As observed in section 5.1.5, the first 14 m from the impact side are characterized by higher heat losses, due to the relatively high speed of the external air around the receiver. Only in this small portion of the receiver length, the influence of the wind on the receiver performance is appreciable. Overall, the heat losses and the thermal

efficiency in the case of wind along the collector axis are  $\sim 6\%$  higher than those in the absence of wind. Moving to



the evacuated tube, Figure 37 and

Figure 38 show that the heat losses and thermal efficiency in case of wind across or along the collector correspond approximately to those obtained in the absence of wind at any location along the receiver. This is because in the evacuated configuration at the CPC shielding effect is added the effect of the strong decoupling between the absorber tube and the glass envelope, which is lapped by the external air flow. Also the peak due to the wind along the collector in the region close to the leading edge, is not evident anymore, as already noticed in section 5.1.5.



According to

Figure 38, the evacuated configuration behaves better than the simply encapsulated one, especially in case of wind. However, the reduction of the receiver efficiency is not dramatic; it leads to a reduction of the oil temperature increase along the hydraulic loop of about 5% in the worst case (from 152 K to 145 K, not shown).

The fact that the differences in the thermal performance between the evacuated and simply encapsulated tube are not really significant confirms the results obtained by Montes et al. (2017), who concluded that only a modest benefit can be obtained adopting an evacuated tube at low temperatures, as the ones considered here.

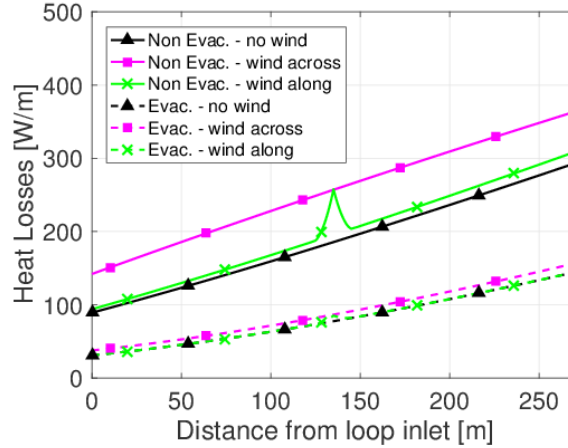


Figure 37 – Computed heat losses from the absorber tube along the receiver length for the simply encapsulated (solid lines) and the evacuated (dashed lines) tube in the absence of wind (triangles), wind across the receiver (squares) and wind along the receiver axis (x-marks), respectively.

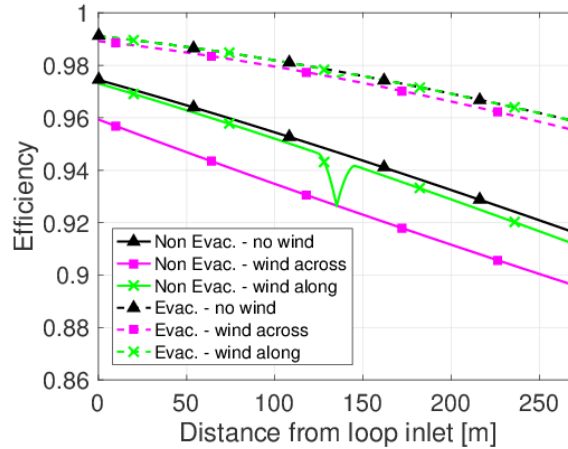


Figure 38 – Computed thermal efficiency along the receiver length for the simply encapsulated (solid lines) and the evacuated (dashed lines) tube in the absence of wind (triangles), wind across the receiver (squares) and wind along the receiver axis (x-marks), respectively.

## 7 Conclusions

In this paper different models (1D, 2D and 3D) have been developed and applied to the analysis of heat losses from a Fresnel receiver equipped with a CPC, in the two configurations of evacuated and simply encapsulated receiver.

First, an optical analysis has been performed by means of a Monte Carlo ray tracer in order to determine the optical performance of the collector and the heat absorbed by the receiver. On an annual base, the optical efficiency of the LFC considered here is about 51%, although this value is probably quite optimistic due to the approximation introduced.

A reference day and time (March 21, GMT 12:00) has been investigated in detail considering different wind directions (along and across the receiver axis) as well as the case of absence of wind. The results indicate that the wind effect on the receiver performance is absolutely negligible for the evacuated tube, which presents a strong thermal decoupling between the glass cover and the absorber tube. Hence, a change in the convective heat transfer condition between the glass cover and the external ambient does not affect the heat loss by the absorber tube. The worsening in the receiver performance in the case of a simply encapsulated tube is modest, likely because of the screening action of the CPC. Furthermore, in case of wind blowing along the collector, the effect of the wind is relevant only for a small portion of the receiver tube, close to the “entry” region, which results in a total increase of the heat losses of only ~6%.

The analysis of the reference day and time also leads to the conclusion that the evacuated tube perform only slightly better than the simply encapsulated one. In fact, due to the relatively low temperatures reached by the receiver in the system analyzed, the heat losses are a very small share of the absorbed heat in both receiver configurations. However, the performance difference between the two receiver configurations depends significantly on the heat absorbed by the absorber tube, which is in turn a function of the DNI level and of the optical efficiency that changes with the sun position. Particularly, it has been noticed that the thermal efficiency decreases with the absorbed heat since the heat losses are quite constant for a given oil temperature, but this reduction is much more pronounced in the case of the simply encapsulated tube. On an annual base, the benefit of using an evacuated tube can be approximately quantified as  $\sim 10\%$  increase of the thermal efficiency, at least in the case of wind blowing across the receiver axis.

The good thermal efficiencies reached by the receivers analyzed here also depend on the excellent behavior of the selective coating adopted (CERMET) that ensures a very low surface emissivity. Using a non-selective coating, like the Pyromark 2500, leads to a drastic increase of the radiative heat losses ( $\sim 7$  times higher) that lowers the thermal efficiency.

The results obtained in this paper will provide the baseline for further economic analysis aimed to establish if the gain in efficiency obtained with the evacuated tube justifies the additional manufacturing costs related to the evacuation of the tube. In addition, as a future perspective, the sensitivity analysis with respect to the wind intensity is planned to be extended considering also higher wind speeds, which should lead to more significant heat losses.

## References

- AK Steel, 2016. 321 Stainless Steel [WWW Document]. URL [http://www.aksteel.com/pdf/markets\\_products/stainless/austenitic/321\\_Stainless\\_Steel\\_DS\\_201512.pdf](http://www.aksteel.com/pdf/markets_products/stainless/austenitic/321_Stainless_Steel_DS_201512.pdf) (accessed 12.12.16).
- Bernhard, R., Laabs, H., Lalaing, J. De, 2008. Linear Fresnel collector demonstration on the PSA, Part I—design, construction and quality control, in: 14th International SolarPACES Conference. Las Vegas, pp. 1–10.
- Blanco, M.J., Amieva, J.M., Mancilla, A., 2005. The Tonatiuh Software Development Project: An open source approach to the simulation of solar concentrating systems, in: Proceedings of the ASME Computers and Information in Engineering Division. pp. 157–164.
- Blanco, M.J., Mutuberria, A., Martinez, D., 2010. Experimental validation of Tonatiuh using the Plataforma Solar de Almería secondary concentrator test campaign data, in: 16th SolarPACES Conference. Perpignan, France.
- Canavarro, D., Chaves, J., Collares-Pereira, M., 2014. Simultaneous Multiple Surface method for Linear Fresnel concentrators with tubular receiver. *Sol. Energy* 110, 105–116.
- CD-ADAPCO, 2014. STAR CCM+ User Guide, version 9.02.
- CENER, 2015a. Measurement of transmittance, absorptance and emittance of small Archimede samples. Technical Report No 30.2652.0.
- CENER, 2015b. Optical and thermal characterization of parabolic trough solar receivers. Test Report No. 30.2715.0-3.
- ENEA, 2015. Laboratorio di qualificazione collettori e sistemi solari, Technical Report n° RT.2015.COL183.1.
- Forristall, R., 2003. Heat Transfer Analysis and Modeling of a Parabolic Trough Solar Receiver Implemented in Engineering Equation Solver. Technical Report, NREL/TP-550-34169, National Renewable Energy Laboratory.
- Francis, N.D.J., Itamura, M.T., Webb, S.W., James, D.L., 2002. CFD Calculation of Internal Natural Convection in the Annulus between Horizontal Concentric Cylinders. Sandia National Laboratories Report No. 3132.
- Grena, R., Tarquini, P., 2011. Solar linear Fresnel collector using molten nitrates as heat transfer fluid. *Energy* 36, 1048–1056.
- Haberle, A., Zahler, C., Lerchenmueller, H., Mertins, M., Wittwer, C., Trieb, F., Dersch, J., 2002. The Solarmundo line focussing Fresnel collector. Optical and thermal performance and cost calculations. *Proc. SolarPACES* 1–11.
- Heimsath, A., Cuevas, F., Hofer, A., Nitz, P., Platzer, W.J., 2014. Linear Fresnel Collector receiver: Heat loss and temperatures, in: *Energy Procedia*. pp. 386–397.
- Ho, C.K., Mahoney, A.R., Ambrosini, A., Bencomo, M., Hall, A., Lambert, T.N., 2013. Characterization of Pyromark 2500 Paint for High-Temperature Solar Receivers. *J. Sol. Energy Eng.* 136, 14502.
- Incropera, F.P., DeWitt, D.P., Bergman, T.L., Lavine, A.S., 2012. Fundamentals of Heat and Mass Transfer, sixth. ed,

- Wiley.
- IRESEN, 2016. Green Energy Park [WWW Document]. URL <http://www.greenenergypark.ma> (accessed 12.2.16).
- Lancereau, Q., Rabut, Q., Itskhokine, D., Benmarraze, M., 2015. Wind Loads on Linear Fresnel Reflectors' Technology: A Numerical Study, in: *Energy Procedia*. pp. 116–125. doi:10.1016/j.egypro.2015.03.014
- Menter, F.R., 1994. Two-equation eddy-viscosity turbulence models for engineering applications. *AIAA J.* 32, 1598–1605.
- Mills, D.R., Morrison, G.L., 2000. Compact linear fresnel reflector solar thermal powerplants. *Sol. Energy* 68, 263–283.
- Moghimi, M.A., Craig, K.J., Meyer, J.P., 2015. A novel computational approach to combine the optical and thermal modelling of Linear Fresnel Collectors using the finite volume method. *Sol. Energy* 116, 407–427.
- Montes, M.J., Abbas, R., Muñoz, M., Muñoz-Antón, J., Martínez-Val, J.M., 2017. Advances in the linear Fresnel single-tube receivers: Hybrid loops with non-evacuated and evacuated receivers. *Energy Convers. Manag.* 149, 318–333.
- Montes, M.J., Barbero, R., Abbas, R., Rovira, A., 2016. Performance model and thermal comparison of different alternatives for the Fresnel single-tube receiver. *Appl. Therm. Eng.* 104, 162–175.
- Morin, G., Dersch, J., Platzer, W., Eck, M., Häberle, A., 2012. Comparison of Linear Fresnel and Parabolic Trough Collector power plants. *Sol. Energy* 86, 1–12. doi:10.1016/j.solener.2011.06.020
- Österholm, R., Pålsson, J., 2014. Dynamic modelling of a parabolic trough solar power plant Parabolic trough and other concen-. *Proc. 10th Int. Model.* 1057.
- Qiu, Y., He, Y.L., Cheng, Z.D., Wang, K., 2015. Study on optical and thermal performance of a linear Fresnel solar reflector using molten salt as HTF with MCRT and FVM methods. *Appl. Energy* 146, 162–173.
- Qiu, Y., He, Y.L., Wu, M., Zheng, Z.J., 2016. A comprehensive model for optical and thermal characterization of a linear Fresnel solar reflector with a trapezoidal cavity receiver. *Renew. Energy* 97, 129–144.
- Raccurt, O., Disdier, A., Bourdon, D., Donnola, S., Stollo, A., Gioconia, A., 2015. Study of the Stability of a Selective Solar Absorber Coating under Air and High Temperature Conditions, in: *Energy Procedia*. pp. 1551–1557.
- Sabatelli, V., Marano, D., Contento, G., Bruno, A., Ebolese, A., Del Col, D., Quaggia, M., Bortolato, M., Bortolin, S., Padovan, A., 2013. ENEA, Report RdS/2013/092 - Sperimentazione e qualificazione di componenti solari a concentrazione per applicazioni a media temperatura. [WWW Document]. URL [http://www.enea.it/it/Ricerca\\_sviluppo/documenti/ricerca-di-sistema-elettrico/climatizzazione-rinnovabili/2012/rds-2013-092.pdf](http://www.enea.it/it/Ricerca_sviluppo/documenti/ricerca-di-sistema-elettrico/climatizzazione-rinnovabili/2012/rds-2013-092.pdf) (accessed 12.12.12).
- Sahoo, S.S., Varghese, S.M., Suresh Kumar, C., Viswanathan, S.P., Singh, S., Banerjee, R., 2013. Experimental investigation and computational validation of heat losses from the cavity receiver used in linear Fresnel reflector solar thermal system. *Renew. Energy* 55, 18–23.
- Sait, H.H., Martinez-Val, J.M., Abbas, R., Munoz-Anton, J., 2015. Fresnel-based modular solar fields for performance/cost optimization in solar thermal power plants: A comparison with parabolic trough collectors. *Appl. Energy* 141, 175–189.
- Shih, T.H., Liou, W.W., Shabbir, A., Yang, Z., Zhu, J., 1994. A new k-epsilon eddy viscosity model for high Reynolds number turbulent flows: Model development and validation. *Comput. Fluids* 24, 227–238.
- Singh, P.L., Sarviya, R.M., Bhagoria, J.L., 2010. Heat loss study of trapezoidal cavity absorbers for linear solar concentrating collector. *Energy Convers. Manag.* 51, 329–337. doi:10.1016/j.enconman.2009.09.029
- Soltigua, 2015. Technical report: 1MWe CSP-ORC pilot plant, solar field process description. Report Number: S-F14ET001-M-B-A-2602-C.
- Weerasinghe, R., Hughes, T.P., 2015. CFD Modelling of Thermo-electric Devices for Thermal Management in Downhole Tools, in: *21st INTERNATIONAL WORKSHOP on Thermal Investigations of ICs and Systems (THERMINIC)*. pp. 1–4.